(2)

Technical Report 1479
January 1992

Prototype Superconducting Planar Transformers Using High-T_c Thin and Thick Films

W. C. McGinnis
J. S. Briggs
T. E. Jones
L. J. Johnson

NAVAL OCEAN SYSTEMS CENTER

San Diego, California 92152-5000

J. D. FONTANA, CAPT, USN
Commander

R. T. SHEARER
Technical Director

ADMINISTRATIVE INFORMATION

This work was performed for the Office of the Chief of Naval Research (OCNR-10P), Independent Exploratory Development Programs (IED), Arlington, Virginia 22217-5000, under program element 0602936N and project RV36I21. The work was performed by members of the Materials Research Branch, Code 573, Naval Ocean Systems Center, San Diego, California 92152-5000.

Released by
J. C. Hicks, Head
Materials Research
Branch

Under authority of
R. H. Moore, Head
Applied Sciences
Division

MA

DISCLAIMER NOTICE

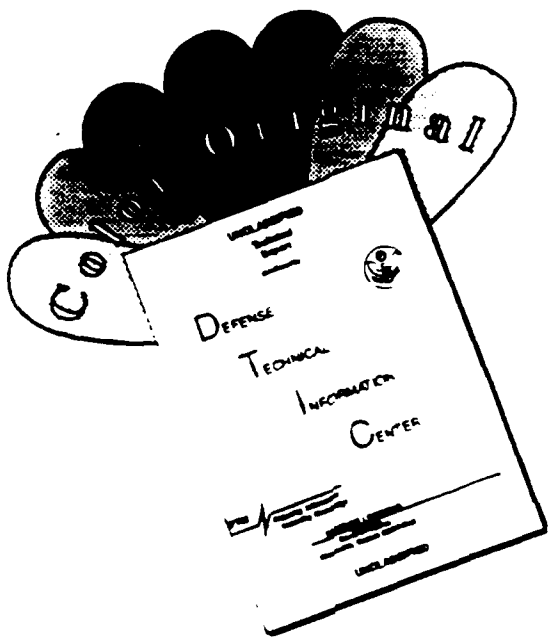

THIS DOCUMENT IS BEST QUALITY AVAILABLE. THE COPY FURNISHED TO DTIC CONTAINED A SIGNIFICANT NUMBER OF COLOR PAGES WHICH DO NOT REPRODUCE LEGIBLY ON BLACK AND WHITE MICROFICHE.

SUMMARY

OBJECTIVE

To develop a prototype version of an on-chip electrical transformer using high transition temperature superconducting films.

RESULTS

Two approaches for making high-T_c films for use in a superconducting planar transformer have been pursued: melt-processing of thick films and sputter deposition of thin films. A prototype transformer has been made and characterized, for demonstration purposes, using each approach.

The crystalline and superconducting properties of melt-processed $Bi_2Sr_2CaCu_2O_8$ thick films were investigated as a function of melt temperature (895°C to 950°C) and cooling rate (0.1°C/min to 240°C/min) from the melt-processing temperature. The films with the best superconducting properties were melted at 900°C, and then rapidly cooled from that temperature. Thin films of $YBa_2Cu_3O_7$ were deposited by rf diode, off-axis sputtering, using both *in situ* and *ex situ* techniques. The properties of postannealed, or *ex situ*, films were optimized by heating the films to about 900°C in Ar, switching to O_2 and annealing for one hour, and quickly cooling to a lower temperature for the remainder of the process.

A prototype thick film transformer was made by melting $Bi_2Sr_2CaCu_2O_8$ powder on an MgO substrate. The film was patterned in the form of two concentric square loops by scribing after melt-processing. A similar square loop transformer was made using two *ex situ* processed thin films of $YBa_2Cu_3O_7$ that were sandwiched back-to-back. Both transformers were operated, with the films in the superconducting state, at frequencies ranging from 1 kHz to 100 kHz. The thick film transformer was operated at temperatures up to 77 K, and at currents up to 1 A.

CONCLUSIONS

Planar transformers made from high-T_c films have been demonstrated with two prototype devices. Practical microelectronic transformers and other inductive devices will require high-quality films as well as the ability to deposit multiple superconducting and insulating layers.

CONTENTS

FIGURES

TABLES

1. INTRODUCTION

A compact, shielded on-chip transformer would eliminate the need for bulky, energy-consuming, iron-core, wire-wound transformers that produce unwanted electromagnetic interference and noise. Ideally, such a device would have a planar geometry and be in the form of magnetically coupled films that (1) could carry large currents to enhance the magnetic coupling, (2) have low resistance to minimize Joule-heating losses, (3) be easily incorporated as part of an integrated circuit, and (4) be electromagnetically isolated from the rest of the circuit. The perfect material for this application is a superconductor. Below its critical temperature, T_c, the dc resistance of a superconductor is zero, eliminating any heating problems. The ac resistance, though not zero, can be very small, even at gigahertz frequencies. In addition, the ability of a superconductor to exclude magnetic flux means that this type of device can be isolated from the remainder of the circuit with superconducting film overlayers.

The discovery in 1987 (Wu et al., 1987) of superconductors with transition temperatures above liquid nitrogen temperature (77 K) made the practical implementation of a superconducting planar transformer possible. High-T_c superconductors include materials such as $YBa_2Cu_3O_7$ (T_c = 90 K), $Bi_2Sr_2CaCu_2O_8$ (T_c = 80 K), $Bi_2Sr_2Ca_2Cu_3O_{10}$ (T_c = 105 K), and $Tl_2Ca_2Ba_2Cu_3O_{10}$ (T_c = 125 K). Two approaches for making films for use in a prototype superconducting transformer have been pursued in the present study: melt-processing of thick $Bi_2Sr_2CaCu_2O_8$ films and sputter deposition of thin $YBa_2Cu_3O_7$ films. The next two sections describe the experimental techniques used and the properties of the films produced. The characteristics of prototype transformers made from these films are reported in section 4.

2. $Bi_2Sr_2CaCu_2O_8$ THICK FILMS

2.1 INTRODUCTION

Numerous research groups have investigated melt-processing or texturizing techniques (Jin et al., 1988; Salama et al., 1989; Neumüller and Ries, 1989; Peuckert et al., 1989; Zhu et al., 1988; Spann et al., 1990) as a way of improving the critical current density J_c of high-transition-temperature superconductors such as $YBa_2Cu_3O_7$ and $Bi_2Sr_2CaCu_2O_8$. J_c is maximized in these highly anisotropic materials by aligning the individual single-crystal grains with each other so that current flows parallel to the copper-oxygen planes. The crystal unit cell is typically ortho-rhombic, with a c-axis spacing 2 to 7 times that of an approximately equal a-axis and b-axis spacing. These elongated unit cells bond to form flat platelets whose flat surface is parallel to

the a-b (copper-oxygen) planes. The platelet-like crystals, given the opportunity, will lie flat against each other. Reasonably good alignment can be produced by simply pressing the powder. Such alignment has been observed by x-ray diffraction measurements of pressed pellets (Huang et al., 1988) and even of powder that has been finger-pressed on a microscope slide. C-axis alignment has also been enhanced by using a strong magnetic field to align the magnetic rare-earth ions (R) in $RBa_2Cu_3O_7$ samples (Farrell et al., 1987). An even more effective alignment technique is to melt the material and then let it solidify. The degree of alignment will depend on the cooling rate and other conditions.

Although melt-processing produces highly oriented samples, it can have the possible drawback of changing the phase make-up of the sample. The high-T_c ceramic superconducting compounds contain four, five, or more elements that can be redistributed into a number of other compounds upon solidification from the melt of the parent compound. For example, the Bi-Sr-Ca-Cu-O family of superconductors includes phases with the nominal compositions $Bi_2Sr_2CuO_6$, $Bi_2Sr_2CaCu_2O_8$, and $Bi_2Sr_2Ca2Cu_3O_{10}$ (Tarascon et al., 1988). In addition, non-superconducting compounds such as cuprates of Ca and Sr can form. The superconducting properties of the sample are generally degraded by the presence of these unwanted phases and compounds (although very finely dispersed impurities or defects can increase flux pinning and give higher J_c (Murakami et al., 1989; Umezawa et al., 1987)). It can be important, therefore, to maintain the phase purity of melted samples while achieving alignment of the superconducting planes.

This portion of the project compared the phase make-up, crystalline alignment, surface morphology, and superconducting properties of thick $Bi_2Sr_2CaCu_2O_8$ films melt-processed at about 10 to 15°C above the melting temperature (approximately 885°C) of $Bi_2Sr_2CaCu_2O_8$ with those of films melted at about 65°C above that temperature. These properties were also studied as a function of cooling rate (from a few °C/sec to a few °C/hr). The phase purity and crystalline alignment of the samples was characterized by x-ray diffraction, while the surface morphology was studied by scanning electron microscopy (SEM). Resistance versus temperature measurements and transport critical current density as a function of temperature and magnetic field are also reported.

2.2 EXPERIMENTAL PROCEDURES

Before making the thick films, $Bi_2Sr_2CaCu_2O_8$ powder was prepared by solid state reaction, nominally as follows. Stoichiometric amounts of Bi_2O_3, $SrCO_3$, $CaCO_3$, and CuO powders, all at least 99.999% pure, were mixed and ground together. The mixture was calcined at 840°C for 36 hours. The material was then reground and processed at 848°C for 40 hours. All processing was done in air. The powder used for the thick films was obtained by grinding the resulting

material. Pellets pressed from this powder and sintered at 850°C for 20 hours in air had a zero resistance transition temperature of 78 K. X-ray diffraction measurements showed no indication of the $Bi_2Sr_2CuO_6$ or $Bi_2Sr_2Ca_2Cu_3O_{10}$ superconducting phases.

Several candidate substrate materials were used to make melt-processed films at 950°C, including polycrystalline Al_2O_3 and single crystals of MgO, yttria-stabilized ZrO_2, and Si. $Bi_2Sr_2CaCu_2O_8$ showed substantial reaction with Al_2O_3, and very strong reaction with Si. No visible reaction was observed with the other two substrate materials, and both produced films with sharp superconducting transitions at about 80 K. The best films were obtained using the MgO substrates, however, because the films did not adhere well to the ZrO_2 substrates. Therefore, MgO was chosen as the substrate material for this study. All of the films described below were melted on single crystal substrates of (100) oriented, polished MgO.

The $Bi_2Sr_2CaCu_2O_8$ powder described above was thoroughly ground and mixed with a small amount of liquid (either methanol or polyglycol) to form a spreadable paste. The mixture was spread evenly over a substrate with a razor blade or by screen-printing. The thickness of this coating determined the ultimate film thickness. The samples were placed in a furnace, heated from room temperature to 200°C, and held there for one hour to remove the carrier liquid. The temperature was then increased at 5°C/min to the melt-processing temperature, T_{melt}, and held at that temperature for 30 minutes to melt the $Bi_2Sr_2CaCu_2O_8$ powder. The films were cooled to 850°C at a given cooling rate, held there for 6 hours, and cooled at 5°C/min to room temperature. All of this processing was done with the samples in air. The temperatures listed above were measured with a Pt-10% Rh (type S) thermocouple protected by an alumina tube and placed adjacent to the sample in the tube furnace. The samples were positioned in the center of the single zone furnace where the temperature is uniform to within 1°C over a distance of about 6 cm.

All films were characterized by x-ray diffraction, using a Rigaku RU-200B diffractometer with Cu-Kα radiation, and by four-probe resistance versus temperature measurements, using a closed-cycle refrigerator. Some films were scribed in a block "S" pattern for critical current density measurements. A 2 mm wide by 4 mm long, low-critical-current section (the middle part of the "S") was formed by scribing two 7 mm long lines from opposite sides of the 10 mm × 10 mm substrate, with a separation distance between the two lines of 2 mm. The maximum self-field per unit of current for this configuration is estimated to be 0.4 mT/A. The width of the weak link in the center of the film was measured with a magnifying scale, and the film thickness was determined with a micrometer. Low-resistance contacts were made to the other (high-critical-current) sections of the film by heating silver paint pads at 800°C in air for two hours, and then indium-soldering wires to the pads. The current–voltage characteristics were obtained using a previously described pulsed-current technique (McGinnis et al., 1990).

A series of films (using polyglycol as a carrier liquid) were melted at 900°C and cooled at rates of 240°C/min (step-cooled from T_{melt}), 1°C/min, and 0.1°C/min. After scribing for J_c measurements, these films had weak-link cross sections of 0.29, 0.34, and 0.12 mm^2, respectively (with corresponding film thicknesses of 146, 179, and 131 μm, and sample numbers FCS-66, FCS-67, and FCS-76). For comparison, other films were processed in the same way but with $T_{melt} = 950°C$. Of these latter films, only the step-cooled sample (FCS-75) produced a reasonably smooth, uniform-looking film, and therefore only that film was characterized. The weak-link cross section of this 231 μm thick film after scribing was 0.38 mm^2.

To compare the properties of a film with and without the as-melted surface intact, a 390 μm thick film with $T_{melt} = 895°C$ (methanol carrier liquid, cooling rate = 1°C/min, sample number FCS-51) was thinned down to a thickness of 154 μm using 600-grit fine grinding paper. J_c in zero applied magnetic field was measured at various temperatures in the closed-cycle refrigerator both before and after thinning the film. The critical current was determined with a 10 μV/cm electric field criterion. The cross-sectional area of the weak link was 0.82 mm^2 for the as-melted film, and 0.32 mm^2 for the thinned film. J_c(4.2 K) was measured again, with the thinned film immersed in liquid helium, in magnetic fields up to 8 T, both with the film perpendicular and parallel to the field. For each field orientation, the current flow was perpendicular to the field. The data were collected in ever-increasing magnetic fields to avoid trapped flux or hysteresis effects.

2.3 RESULTS AND DISCUSSION

The x-ray diffraction spectrum for one of the films melted at 900°C is shown in figure 1. Nearly all of the peaks are identified as (0 0 ℓ m) peaks, with $\ell + m = 2n$, indicating fairly strong c-axis alignment. The $m = 0$ peaks are main reflections, while the $m = \pm 1$ peaks are due to first-order satellite reflections (Onoda et al., 1988) resulting from the modulated structure (Calestani et al., 1989) of this compound. The intensity is plotted on a square root scale in order to bring out the low-intensity peaks. All of the films melted at 900°C or below show similar c-axis alignment, varying somewhat with cooling rate. The relative degree of alignment and its dependence on cooling rate is indicated by the x-ray rocking curve results listed in table 1. Blank entries in the table indicate the lack of a well-defined rocking curve peak.

Films melted at 950°C, as well as some of those melted at 900°C, contain both the $Bi_2Sr_2CaCu_2O_8$ and $Bi_2Sr_2CuO_6$ phases. An indication of the relative amount of the two phases in the 900°C-melted films is presented in figure 2, which shows the (0 0 2 0) peak region. Only for the film step-cooled from 900°C is $Bi_2Sr_2CuO_6$ undetected in the x-ray spectrum.

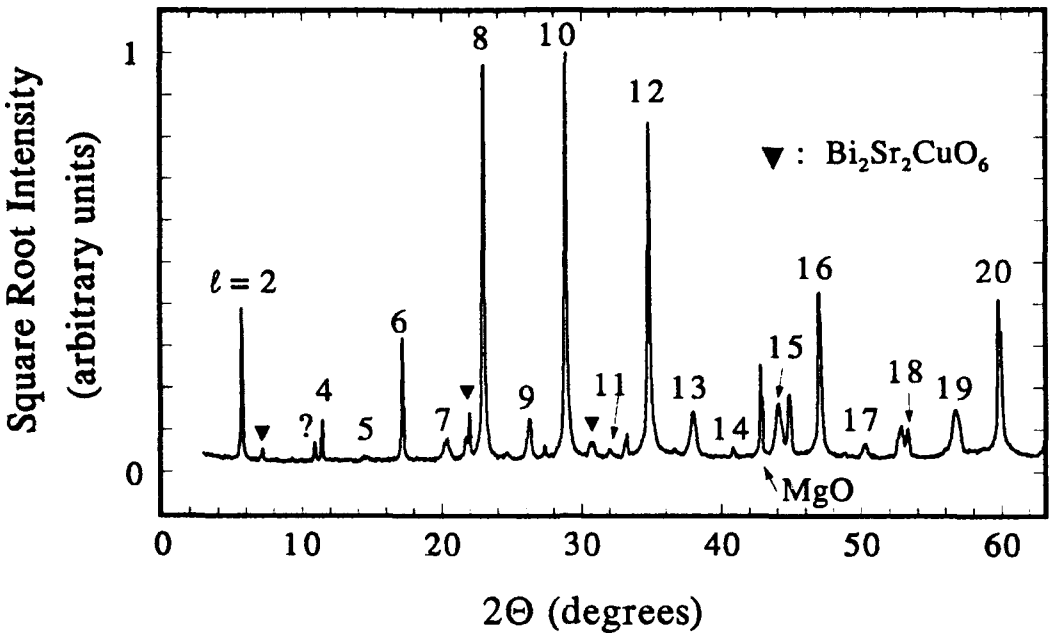

Figure 1. X-ray diffraction spectrum of 900°C-melted $Bi_2Sr_2CaCu_2O_8$ film cooled at 0.1°C/min. $Bi_2Sr_2CaCu_2O_8$ (0 0 ℓ m) peaks are labeled with the ℓ value.

Table 1. Full width half maximum (FWHM) of rocking curves taken about the (0 0 6 0) and (0 0 8 0) peaks of the 900°C-melted films and of the starting $Bi_2Sr_2CaCu_2O_8$ powder.

Sample	Cooling rate (°C/min)	FWHM about (0 0 6 0)	FWHM about (0 0 8 0)
FCS-76	0.1	3.91°	----
FCS-67	1	5.52°	5.82°
FCS-66	240	6.80°	7.84°
starting powder	---	----	9.86°

The surface of the film melted at 895°C had a shiny, glass-like appearance. However, it was not known if the c-axis alignment observed in diffraction measurements was localized to the surface layer or if it extended throughout the bulk of the film. To answer this question, the surface was removed as described above and another diffraction spectrum obtained. This spectrum is shown on a linear intensity scale in figure 3 for mid-range values of 2θ, along with the spectrum of $Bi_2Sr_2CaCu_2O_8$ powder from the batch used to make the film. The relative intensities of the spectra have been adjusted so that the non-(0 0 ℓ m) peaks are approximately equal in height. Although the c-axis alignment is not as complete as in the as-melted film (with

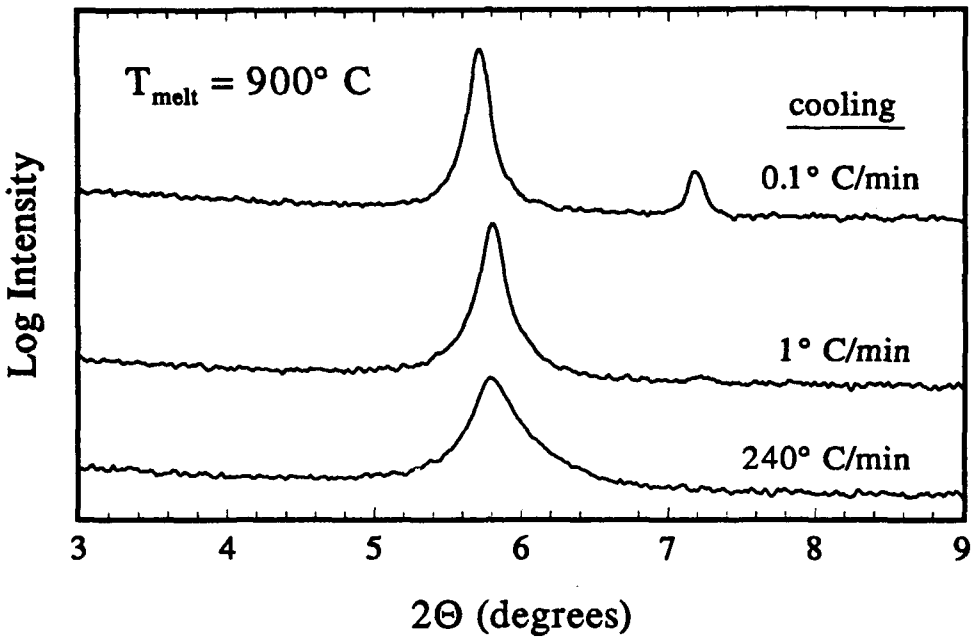

Figure 2. X-ray diffraction spectra for 900°C-melted films with cooling rates shown. The (0 0 2 0) $Bi_2Sr_2CaCu_2O_8$ peak is at 5.7°, and that of $Bi_2Sr_2CuO_6$ is at 7.2°.

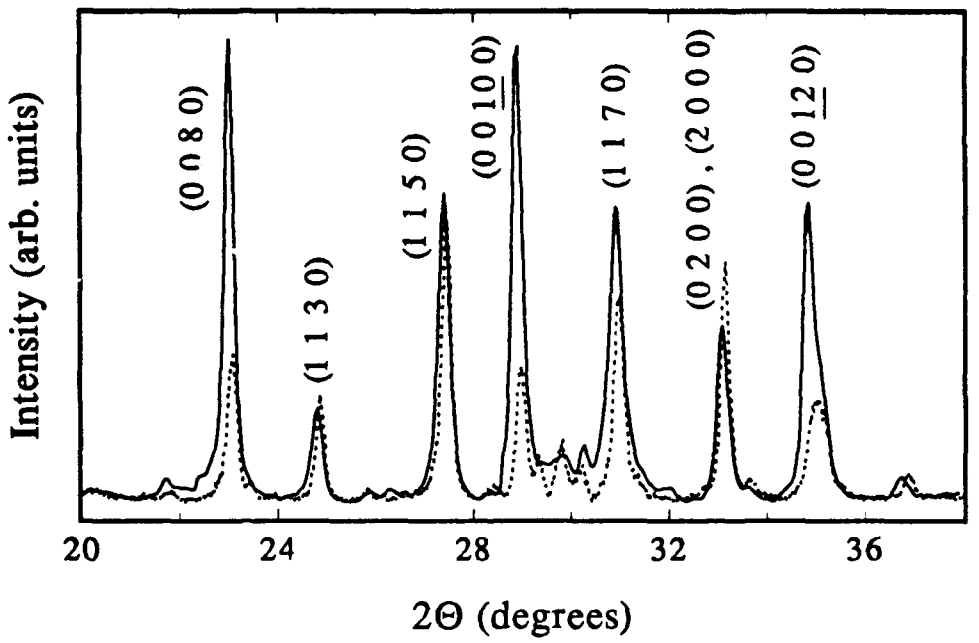

Figure 3. X-ray diffraction spectra of thinned, 895°C-melted $Bi_2Sr_2CaCu_2O_8$ film (solid line) and $Bi_2Sr_2CaCu_2O_8$ starting powder (dashed line).

x-ray spectrum similar to that in figure 1), the (0 0 8 0), (0 0 $\underline{10}$ 0), and (0 0 $\underline{12}$ 0) peaks still show significant enhancements compared to other peaks.

The resistance versus temperature characteristics typical of these films are shown in figure 4. Because the processing was done in air, the zero-resistance transition temperatures are in the range of 80 to 83 K. By reducing the oxygen pressure during the annealing step at 850°C and subsequent cooling to room temperature, the value of T_c could have been increased to above 90 K (Tallon et al., 1989; Knauf et al., 1991). The resistivity curve of the 900°C, step-cooled film (FCS-66) shown in figure 4 is typical of the films melted at the same temperature, but cooled more slowly.

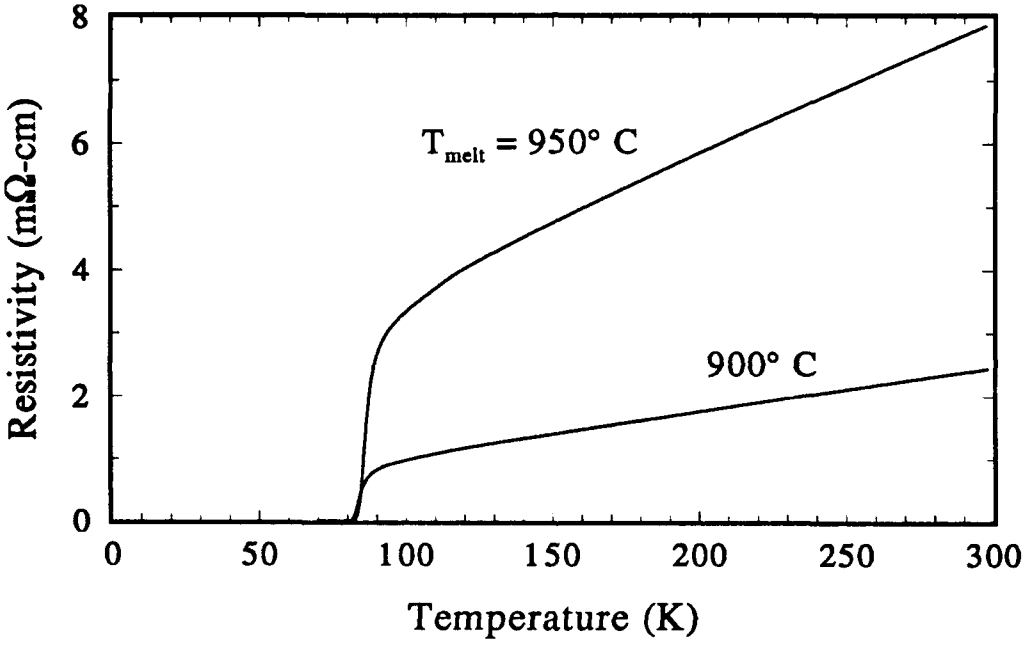

Figure 4. Resistivity versus temperature of $Bi_2Sr_2CaCu_2O_8$ films melted at the temperatures shown and then step-cooled to the annealing temperature of 850°C.

Figure 5 illustrates the variation of J_c with melting temperature and cooling rate, as well as the temperature dependence. The highest J_c is obtained for films melted at 900°C, rather than at 950°C, as seen by comparing the two step-cooled films. This result is consistent with the smaller degree of c-axis alignment for the 950°C film, as evidenced by the lack of (0 0 ℓ m) peak enhancement in its x-ray diffraction spectrum, as well as with the much rougher surface morphology, as seen in figure 6. The differences in morphology might also explain the resistivity characteristics seen in figure 4. Comparison of the three films melted at 900°C in figure 5 clearly shows that the best J_c values are obtained for the more quickly cooled films. This, however, is not the result expected based on c-axis alignment considerations (see table 1), nor

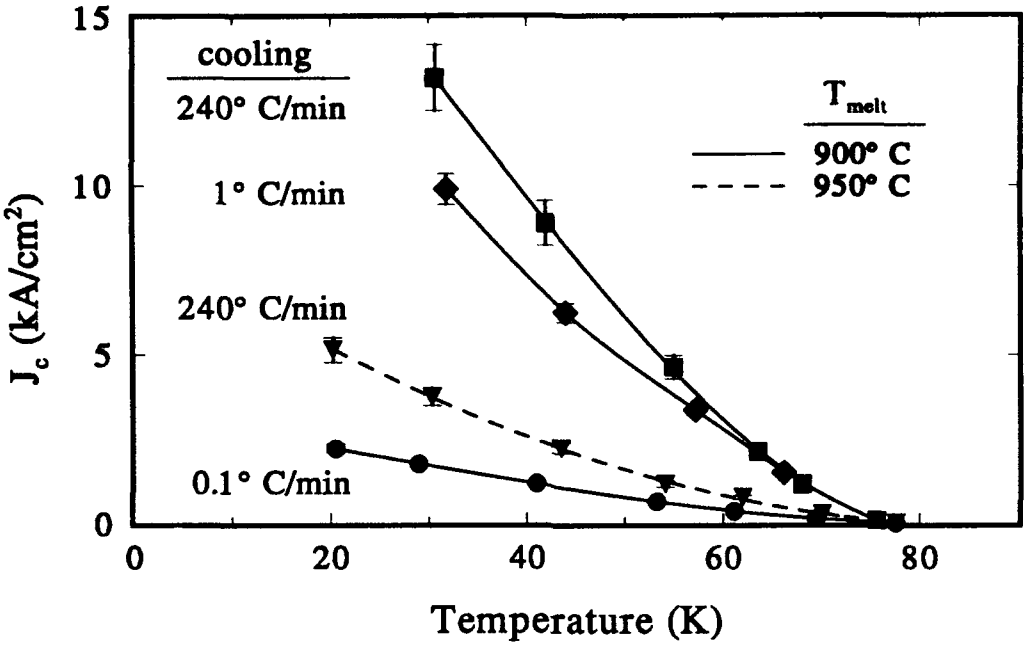

Figure 5. Transport critical current density versus temperature in zero applied field for $Bi_2Sr_2CaCu_2O_8$ films with melt temperatures and cooling rates shown.

is this dependence easily understood in terms of the morphology. Although it may not be clear from figure 6, the slower the cooling rate for the 900°C films, the larger the crystalline features of the film. A comparison of figures 2 and 5, however, indicates that the films with higher J_c values are those with less of the $Bi_2Sr_2CuO_6$ phase.

The temperature dependence of J_c in zero applied field is plotted in figure 7 for the thinned 895°C film. The solid line is a least-square fit of the data to an expression for the critical current density based on the flux-creep model (using the notation of Savvides (1990)):

$$\frac{c}{s} = \exp\left[\frac{-u_o(1+t^2)(1-t^2)}{t}\right] \sinh\left(\frac{s^{1/2}}{t}\right) \qquad (1)$$

where $t = T/T_c$ is the reduced temperature, $u_o kT_c$ is the zero temperature pinning energy, and the dimensionless parameters c and s are given by:

$$c = \frac{E_c \Phi_o^3}{v_o}\left(\frac{a_p}{\beta k T_c}\right)^2$$
$$s(t) = \frac{J(t)\Phi_o^3}{\beta}\left(\frac{a_p}{kT_c}\right)^2 \qquad (2)$$

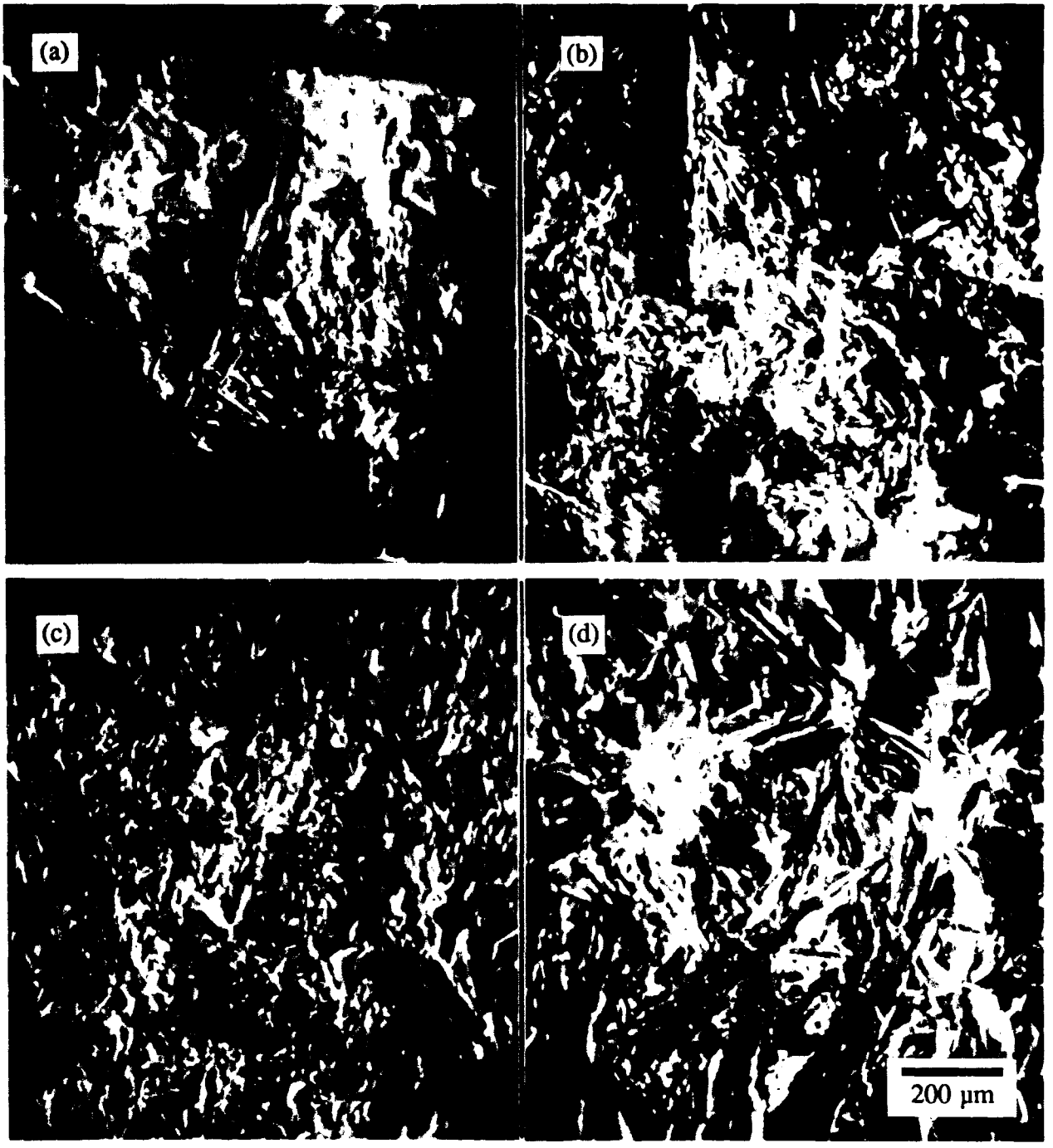

Figure 6. Scanning electron micrographs (all at the same magnification) for 900°C-melted $Bi_2Sr_2CaCu_2O_8$ films cooled at (a) 0.1°, (b) 1°, and (c) 240°C/min, and for a (d) 950°C-melted film cooled at 240°C/min.

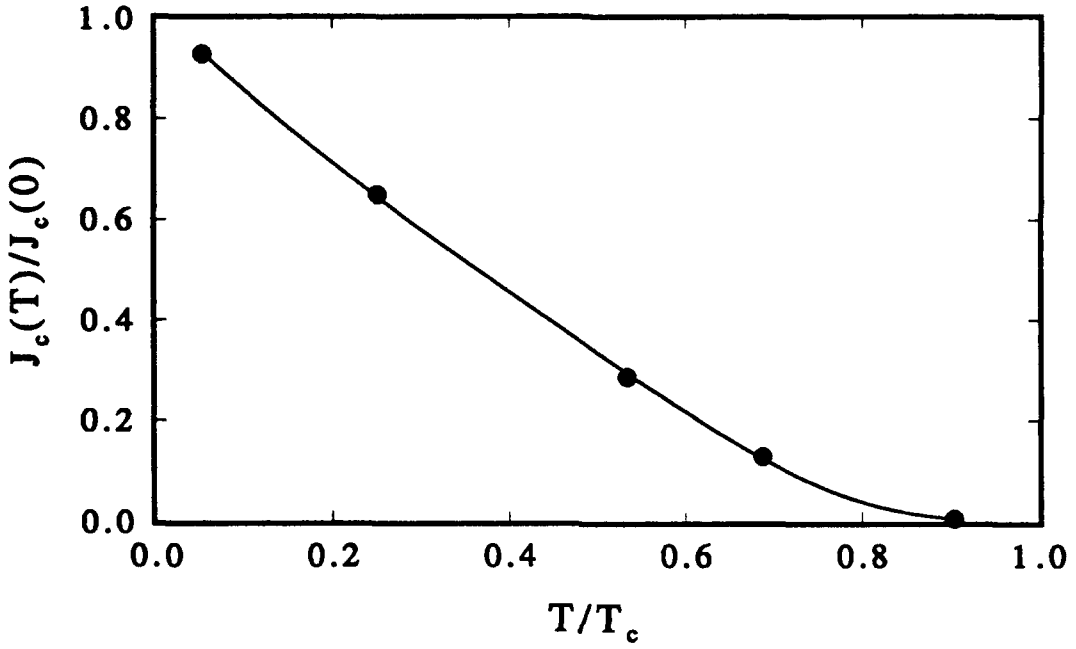

Figure 7. Normalized critical current density versus temperature in zero applied field for the thinned, 895°C-melted $Bi_2Sr_2CaCu_2O_8$ film. The solid line is a fit to equation 1 (see text).

Here, E_c is the electric field criterion defining the critical current, a_p is the distance between pinning sites, the self-field is proportional to J_c and is given by βJ_c, v_o is the flux line drift velocity in the absence of pinning, Φ_o is the flux quantum, and k is Boltzmann's constant. Note that s and J_c are related by $J_c(t)/J_c(0) = s(t)/s(0)$. The sinh (Lorentz force) term of equation 1 assumes a force per unit length of $J_c\Phi_o$ acting on a flux line (or bundle of flux lines) of length a_p over a hop distance equal to the flux line lattice spacing a_o (or na_o for a bundle of n flux lines). The exponential (pinning) term of equation 1 is based on a pinning energy $U \sim H_c^2\xi^2D$, where $H_c(t)$ is the thermodynamic critical magnetic field, $\xi(t)$ is the Ginzburg-Landau coherence length, and D is the diameter of a pinning center (grain boundaries, voids, etc.). A more detailed derivation of equation 1 is given in appendix A. For the fitted line in figure 7, $c = 0.0185$, $u_o = 9.02$, and $s = 79.8$. All of the films characterized here show this flux-creep temperature dependence of J_c. In fact, when the J_c values of all five films of figure 5 are normalized to the respective values at 30 K, all of the data fall on a common curve. Fitting the data to weak-link models (assuming either superconductor/insulator/superconductor or superconductor/normal metal/superconductor junctions at the grain boundaries) gives unsatisfactory results.

The magnetic field dependence of the critical current density of the thinned 895°C film is shown in figure 8. Measurements were performed both with the field parallel and perpendicular

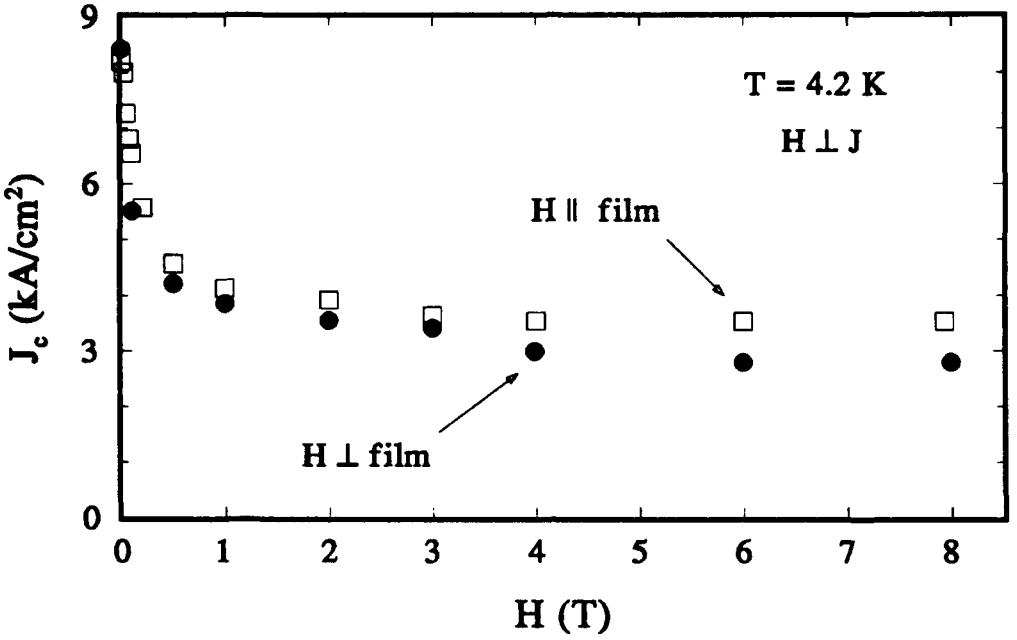

Figure 8. Transport critical current density versus magnetic field of thinned, 895°C-melted $Bi_2Sr_2CaCu_2O_8$ film. The current flow was perpendicular to the magnetic field in both cases.

to the film. Both curves are characterized by J_c undergoing a rapid drop in the low magnetic field region, and then leveling off at fields above 0.5 T or so. The initial decrease in J_c might be attributed to the strong magnetic field dependence of the tunneling current of Josephson junctions formed between weakly linked superconducting grains (Kwak, Venturini, and Ginley, 1987; Peterson and Ekin, 1988). As pointed out by Dew-Hughes (1988), however, J_c should continue to fall toward zero with increasing field. A possible explanation (Ekin, Hart, and Gaddipati, 1990) is that at zero field, the current in these thick films is carried by a parallel combination of high-J_c superconducting material with no weak links (carrying a maximum current I_o through an area A_o) and high-J_c material connected by weak links (carrying a maximum current I_w through an area A_w). The measured critical current density J_c is then the sum of the critical currents divided by the total area, or $(I_o + I_w)/(A_o + A_w)$. As a magnetic field is applied, the tunneling critical current I_w falls off rapidly while I_o decreases more gradually. If the zero field values of I_w and I_o are comparable, then the field dependence shown in the figure is expected. Similar arguments can be made assuming a distribution of grain-to-grain links with strengths ranging from strong to weak (Wang et al., 1988). Such an assembly of grain-to-grain links might consist of a combination of anisotropy-limited (due to relative misorientation of adjacent grains)

links (Ekin et al., 1987) and Josephson-junction-limited (due to normal or insulating barriers between grains) links (Likharev, 1979).

In contrast to the highly anisotropic critical current densities measured (Martin et al., 1989) in single crystals of $Bi_2Sr_2CaCu_2O_8$ ($J_{c\parallel}/J_{c\perp} \approx 10^3$, where $\parallel$ refers to current in the a-b plane), the J_c values shown in figure 8 are only weakly dependent on the orientation of the magnetic field with respect to the film surface (and, therefore, presumably with respect to the c-axis of these partially aligned films). This observation is consistent with the presence of at least some weak links between grains. As suggested by Hampshire et al. (1988), the weak-linked granular nature of the material causes the current to follow a tortuous path among the grains, and so, on the granular scale, the direction of the current with respect to the magnetic field is not constant.

3. $YBa_2Cu_3O_7$ THIN FILMS

3.1 INTRODUCTION

There are two general approaches to producing thin films of $YBa_2Cu_3O_7$ using vapor phase deposition (Somekh, 1990): (1) *in situ* (all processing done in the vacuum deposition chamber) and (2) *ex situ* (part of the processing usually done outside of the growth chamber). In the *in situ* approach, a film is deposited in a partial atmosphere of oxygen onto a substrate heated to between 650 and 800°C. Under these conditions, the film grows in the tetragonal crystal phase of $YBa_2Cu_3O_x$ (with $x \approx 6.2$) as deposited. In the *ex situ* approach, a film is deposited onto a substrate at a temperature less than about 400°C. This low deposition temperature leads to an amorphous Y-Ba-Cu-O film. After deposition, the film is usually removed from the vacuum chamber, and annealed, in oxygen, in a furnace at around 900°C to form tetragonal $YBa_2Cu_3O_x$. After forming this phase, either *in situ* or *ex situ*, the films are slowly cooled in a high partial pressure of oxygen to about 450°C. This step transforms the film's crystal structure from tetragonal to orthorhombic (the superconducting phase). A short anneal at this temperature in oxygen, followed by a slow cool to room temperature, brings the value of x up to near 7.

In either of the above approaches, there are several deposition parameters that can greatly influence the quality of the resulting film. These include the choice of substrate, the substrate temperature during deposition, and the gas species and pressure. The best films have been grown on polished, single-crystal, lattice-matched substrates that do not chemically react with $YBa_2Cu_3O_7$ at the high process temperatures. Commonly used substrates are (100) oriented $SrTiO_3$, Y_2O_3-stabilized ZrO_2, and MgO. The substrate temperature, T_{sub}, is of great importance, particularly for *in situ* films. T_{sub} must be high enough to form the crystalline 123 structure, yet not so high as to promote substrate/film reactions or to cause decomposition of the $YBa_2Cu_3O_x$

phase. T_{sub} also determines the crystalline orientation of the film with respect to that of the substrate (Tanaka and Itozaki, 1989). The films can be amorphous (T_{sub} < 500°C), polycrystalline (500°C < T_{sub} < 650°C), a-axis-oriented (650°C < T_{sub} < 700°C), or c-axis-oriented (T_{sub} > 700°C). These temperature ranges are only approximate, both because of the inherent difficulty in accurately measuring substrate temperatures and because of the dependence of film crystallinity on oxygen pressure (Feenstra et al., 1991). As discussed by Feenstra et al. (1991) and others (Bormann and Nolting, 1989; Hammond and Bormann, 1989), the oxygen partial pressure during deposition and annealing has a dramatic effect on the film's structural and superconducting properties. In addition, the required partial pressure depends on the form (O_2, O_2^+, O, etc.) of oxygen present (Yamamoto et al., 1990). Finally, all of these parameters (substrate, temperature, and oxygen) are interdependent. That is, changing one parameter affects the optimum choices for the other two.

3.2 EXPERIMENTAL PROCEDURES

The deposition equipment available for making $YBa_2Cu_3O_7$ films in this research project was a Varian 980 rf diode sputtering system. A 5 cm diameter $YBa_2Cu_3O_7$ sputtering target was prepared by pressing $YBa_2Cu_3O_7$ powder at 130 MPa at room temperature. The pressed-powder disk was then sintered at 950°C for 12 hours in oxygen, cooled at 1.5°C/min to 550°C, maintained at that temperature for 6 hours, and cooled at 2°C/min to room temperature. Using a hot plate, the sintered disk was attached to a copper backing plate with an alloy of 90% In and 10% Ag. Since the Varian sputterer is normally configured for 15 cm (6 in) diameter targets, a special copper adapter was made to accommodate the smaller target (while maintaining proper ground shielding around the target edges to prevent sputtering of the backing plate).

A number of films were deposited using this sputtering system and target. The sputtering gas consisted of a mixture of 5 mTorr of Ar and 5 mTorr of O_2 (as read using a Varian Millitorr ion gauge, calibrated for N_2, that was placed at the top of the vacuum chamber, near the substrate). Sputtering was performed at a net power between 200 and 400 W, with a target self-bias between 950 and 1450 V. To avoid resputtering of the deposited film (Shah and Carcia, 1987), the substrate was placed off-axis from the target (Terada et al., 1988). In this configuration, the substrate surface is perpendicular to the target surface (with a substrate center to target plane distance of 2.1 cm) and facing the target axis (with a substrate surface to target axis distance of 3.5 cm). A typical deposition rate under these conditions was 30 Å/min.

Ex situ processed films of 1 μm thickness were deposited at ambient temperature. After deposition, the films were removed from the sputtering chamber and annealed in a tube furnace. To achieve uniform heating of the film, the substrate was placed inside a small cylindrical

alumina crucible (with the substrate surface parallel to the axis of the cylinder), which in turn was placed in the tube furnace. The ends of the tube were sealed, and either Ar or O_2 gas was flowed through the tube at a rate of about 0.2 l/min (after first flushing the tube at a higher flow rate). The temperature of the film was measured with a Pt/Pt-6% Rh (type S) thermocouple suspended in the center of the tube.

In situ films approximately 0.25 μm thick were deposited onto substrates heated to between 700 and 800°C. The substrates were first thermally and mechanically attached to small pieces of copper foil using silver paint (baked for a short time at 500°C in Ar). The substrate/foil combination was clamped to a small steel plate, which was radiantly heated by a resistively heated Kanthal wire. The substrate temperature was determined using an alumel-chromel (type K) thermocouple attached to a dummy substrate that was similarly mounted on the steel plate. Immediately after deposition, the O_2 partial pressure was increased to 100 Torr. The substrate temperature was reduced, at a rate of about 25°C/min, to 450°C. The O_2 pressure was then brought up to 760 Torr (1 atm), and the temperature maintained at 450°C for 10 minutes. The film was then cooled at about 5°C/min to room temperature.

3.3 RESULTS AND DISCUSSION

One requirement for high-quality films is that the elemental stoichiometry be within a few percent of the formula values (Chew et al., 1990; Carlson et al., 1990). To check the dependence of stoichiometry on substrate position, a series of unheated alumina substrates were placed at various positions relative to the sputtering target. Y-Ba-Cu-O films were deposited onto these substrates and then chemically analyzed by inductively coupled plasma atomic emission spectroscopy (ICP-AES). The results are shown in table 2, with the film closest to the desired 1:2:3 ratio of Y:Ba:Cu as the first entry. This optimal substrate position was then used for all subsequent film depositions.

The quality of *ex situ* films has been shown to depend, in part, on the furnace atmosphere used during post-deposition annealing. Dubreuil et al. (1989) found that films heated up to the anneal temperature (880°C) in Ar, and then switched to O_2 for the remainder of the processing, had lower resistivities, higher resistance ratios, sharper transitions, and higher transition temperatures than films processed entirely in O_2. Similar results were seen by Escribe-Filippini et al. (1989) and by Ryu et al. (1989). This procedure was therefore adopted for *ex situ* processing of $YBa_2Cu_3O_7$ films in this study.

Several annealing parameters were varied to improve the quality of *ex situ* processed films, including the substrate used, the maximum anneal temperature (T_{anneal}), the time spent at T_{anneal}, and the cooling rate from T_{anneal} to 750°C. Figure 9 shows the normalized resistance versus

Table 2. Y-Ba-Cu-O film stoichiometry dependence on substrate position.

Sample	Substrate position		Atomic ratio		
	Distance to target surface (cm)	Distance to target axis (cm)	Y	Ba	Cu
FCS-102	2.1	3.5	1.000	2.060	3.143
FCS-103	3.7	4.5	1.000	2.233	3.851
FCS-104	2.1	4.5	1.000	2.319	3.217
FCS-105	0.5	4.5	1.000	2.346	3.236
FCS-106	2.1	5.5	1.000	2.245	3.170

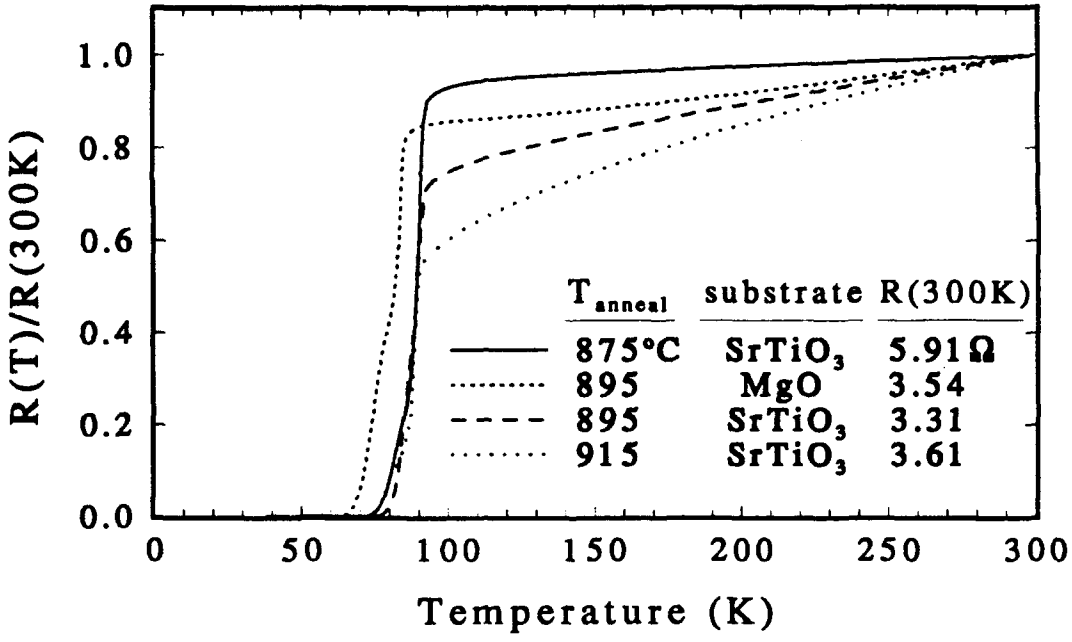

Figure 9. Normalized resistance as a function of temperature for $YBa_2Cu_3O_7$ films, on two different substrates, *ex situ* annealed for one hour at the temperatures shown.

temperature of films processed at various T_{anneal} values, and on two types of substrates. The films on $SrTiO_3$ (FCS-107, FCS-108, and FCS-111 annealed at 875, 895, and 915°C, respectively) showed better resistance characteristics and higher T_c than the one on MgO (FCS-110). The film annealed at 915°C shows a steeper resistance drop from room temperature down to 100 K than the others, but has a pronounced double step in the superconducting transition.

When examined on a magnified resistance scale, the three films on $SrTiO_3$ have essentially the same zero resistance T_c.

The x-ray diffraction spectra of these same films are shown in figure 10. The crystal structure of $YBa_2Cu_3O_7$ is evident in all three samples. Increasing T_{anneal} seems to have two main effects. First, as T_{anneal} is increased, the $YBa_2Cu_3O_7$ (0 0 ℓ) peak heights increase relative to the non-(0 0 ℓ) peaks (see, for example, the (0 0 2) peak at $2\theta \approx 15.2°$), indicative of alignment of the $YBa_2Cu_3O_7$ c-axis perpendicular to the substrate surface. Second, at $T_{anneal} = 915°C$, a second crystal phase appears. This phase, with (0 0 ℓ) peaks marked by ▾ in figures 10 and 11, has a c-axis periodicity of about 14.7 Å and is perhaps related to the so-called "248" phase (Kapitulnik, 1988).

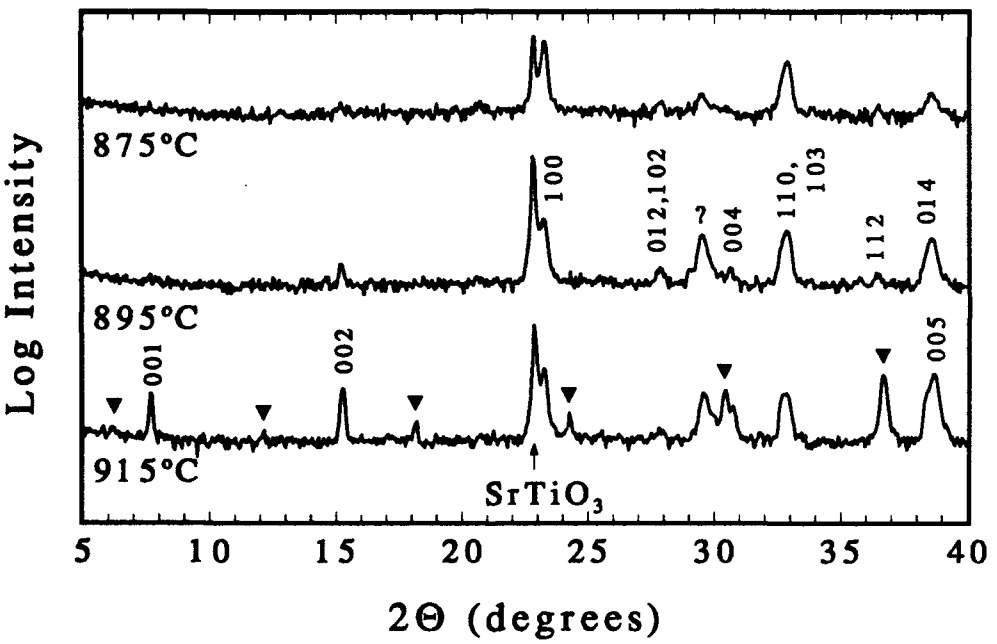

Figure 10. X-ray diffraction spectra for the $YBa_2Cu_3O_7$ films of figure 9 that were deposited on $SrTiO_3$ and *ex situ* annealed at the temperatures shown.

The effect of the time spent at T_{anneal} on the resistive behavior of *ex situ* films is illustrated in figure 11. Also shown is the effect of cool-down rate from T_{anneal} to 750°C. All of the films of this figure were annealed at 915°C. There does not appear to be much difference between the films with regard to their R versus T behavior. The influence of time and cooling rate is more pronounced in the phase make-up of the films, as shown in the x-ray diffraction spectra of figure 12. The content of the second phase referred to above decreases for longer annealing times (see the $2\theta \approx 36.6°$ peaks in figure 12, for example). In addition, diffraction measurements

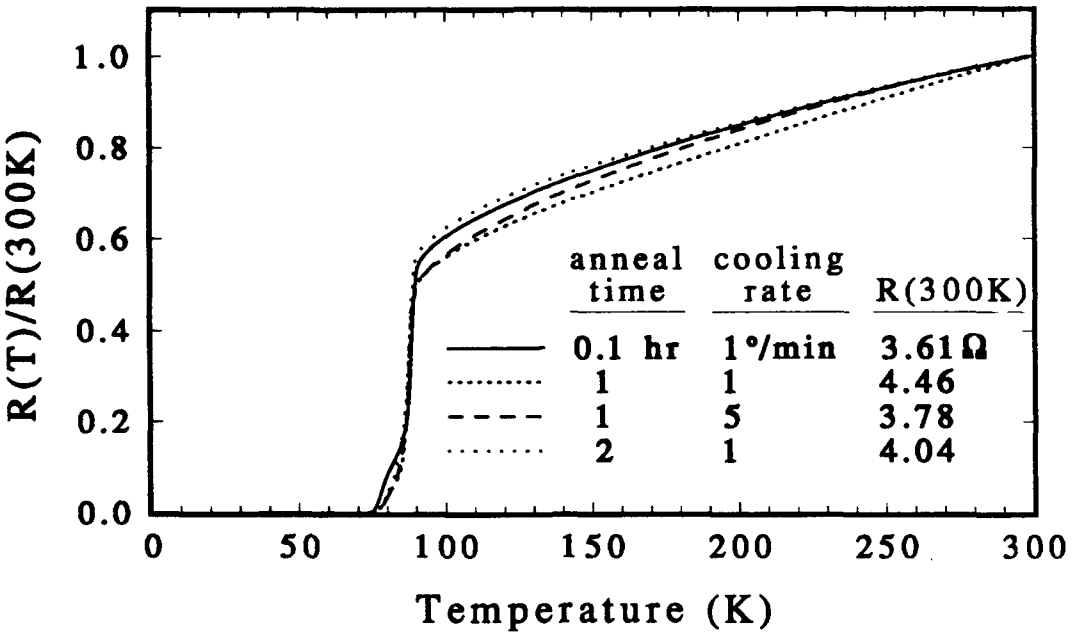

Figure 11. Normalized resistance versus temperature for $YBa_2Cu_3O_7$ films *ex situ* annealed at 915°C for the times shown.

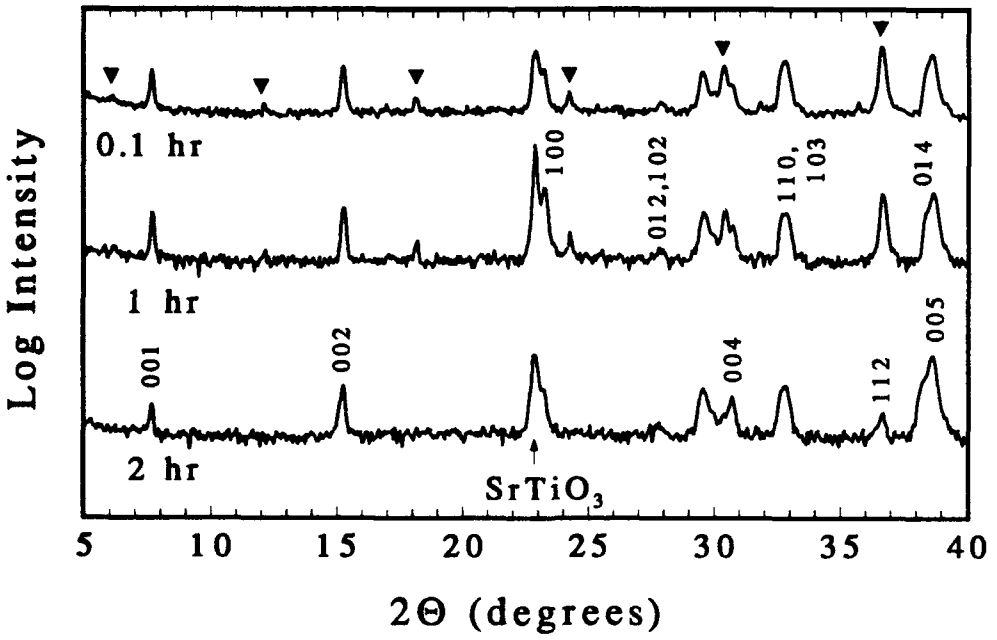

Figure 12. X-ray diffraction spectra for the $YBa_2Cu_3O_7$ films of figure 11 cooled at 1°C/min and maintained at the anneal temperature of 915°C for the times shown.

show that formation of this phase is also favored by slower cooling rates from T_{anneal}.

A number of *in situ* films, on MgO substrates, were also prepared. The effect of deposition temperature on the films' resistive characteristics is shown in figure 13. Films FCS-94, FCS-96, FCS-95, FCS-93, and FCS-97 were processed at substrate temperatures of 700, 735 (see below), 750, 770, and 800°C, respectively. Higher substrate temperatures give higher resistance ratios and transition temperatures, but also produce higher film resistivities. The x-ray diffraction spectra of these films all indicate substantial c-axis alignment. The spectrum of FCS-93, with $T_{sub} = 770°C$, is shown in figure 14. Film FCS-96 was deposited at 700°C, and then annealed *in situ* for 20 minutes in 210 mTorr of O_2. Non-(0 0 ℓ) peaks are observed in the spectrum of this film, but do not appear at all in the spectra of films deposited at higher temperatures. Another effect of temperature observed in the x-ray spectra is reduced lattice constant with higher substrate temperature. As observed by others (Somekh, 1990), this reduction of the c-axis lattice spacing correlates with the increased T_c seen in figure 13.

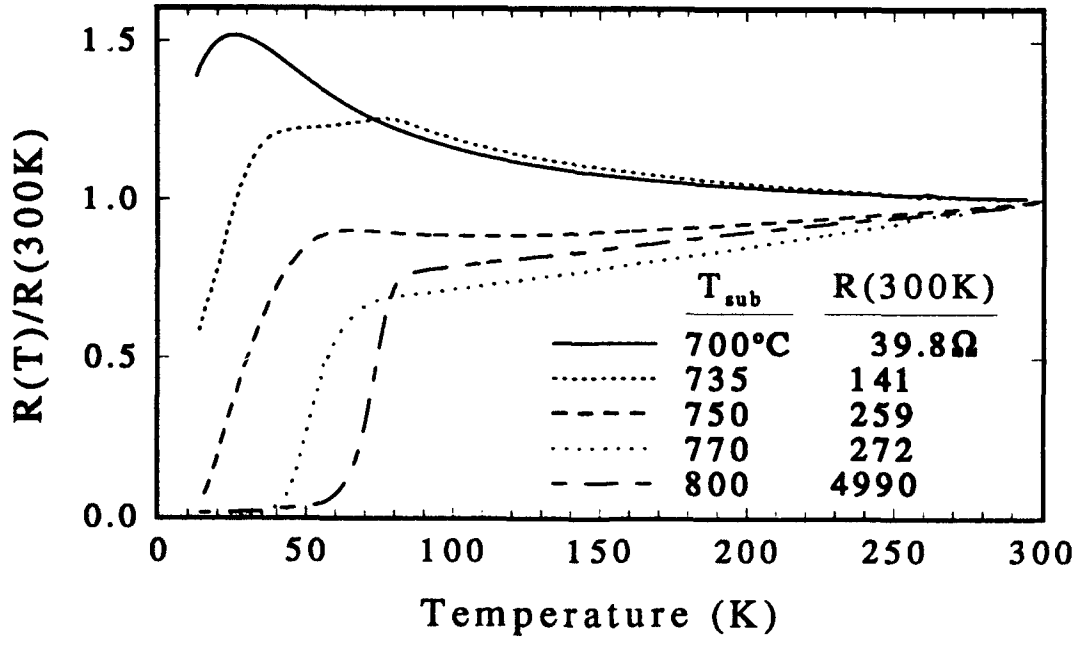

Figure 13. Normalized resistance versus temperature for *in situ* $YBa_2Cu_3O_7$ films deposited at the substrate temperatures shown.

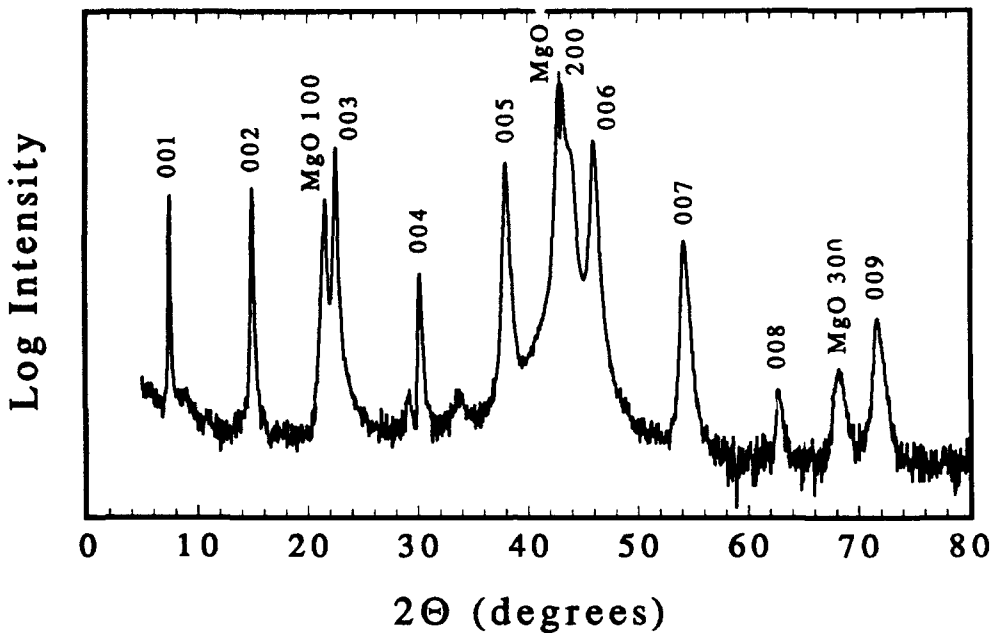

Figure 14. X-ray diffraction spectrum of the *in situ* $YBa_2Cu_3O_7$ film of figure 12 with $T_{sub} = 770°C$.

4. PROTOTYPE TRANSFORMERS

4.1 CALCULATED TRANSFORMER CHARACTERISTICS

Consider two perfectly coupled transformer loops (or coils), each with resistance R and inductance L. In this case, the mutual inductance M is equal to L. Let one loop (the primary) be connected to a sinusoidal current source, and the other (the secondary) be connected to a load resistance R_L. If the current through the primary is*

$$I_p = I_p^o e^{i\omega t} \quad , \tag{3}$$

then the primary and secondary voltages are given by (Anderson and Beeman, 1973)

$$V_p = I_p(R + i\omega L) + I_s(i\omega M) \tag{4}$$

*Complex notation is used here, with $e^x = \cos(x) + i \sin(x)$. The actual currents and voltages are given by the real part of the stated expressions.

$$V_s = I_s(R + i\omega L) + I_p(i\omega M) = -I_s R_L \quad . \tag{5}$$

Here the subscript p refers to the primary, and the subscript s to the secondary. With $R = 0$ for a superconducting transformer (at low enough frequencies), $M = L$, I_p from equation 3, and I_s from equation 5, equation 4 becomes

$$V_p = \frac{\omega L R_L}{\sqrt{R_L^2 + \omega^2 L^2}} I_p^o e^{i(\omega t + \phi)} \quad , \tag{6}$$

where $\phi = \tan^{-1}[R_L/(\omega L)]$. For the case of no load resistor (open secondary), or for $R_L >> \omega L$,

$$V_p = \omega L I_p^o e^{i(\omega t + \pi/2)} \quad . \tag{7}$$

4.2 $Bi_2Sr_2CaCu_2O_8$ THICK FILM TRANSFORMER

A simple prototype $Bi_2Sr_2CaCu_2O_8$ thick film transformer shown in figure 15 along with the $YBa_2Cu_3O_7$ thin film transformer to be discussed in section 4.3, was made as described in section 2.2. The melt temperature was 900°C, and the film was step-cooled after melting. Patterning of this film (FCS-65) was done mechanically by scribing and grinding after melt-processing. The film thickness was 60 μm, and pattern line-width was 1 mm. Silver contact pads for current and voltage connections were baked on as described earlier. The MgO substrate was attached to a thin alumina square using G.E. varnish. Twisted pairs of copper wire were indium-soldered to the silver pads, and secured to the alumina with tape. The alumina square was then attached to a fused quartz disk (2.5 cm diameter, 0.32 cm thick) with Apiezon N-grease, which in turn was N-greased to the copper sample stage of the closed-cycle refrigerator. The purpose of the quartz disk was to ensure an open magnetic flux path between the transformer and the metallic sample stage. One junction of a copper-constantan (type T) differential thermocouple was indium-soldered to a small piece of alumina, which was N-greased to the central portion of the MgO substrate. The other thermocouple junction was attached to the sample stage, whose temperature was measured with a silicon diode thermometer. The differential thermocouple thus provides a measure of the temperature difference between the sample (transformer) and the sample stage.

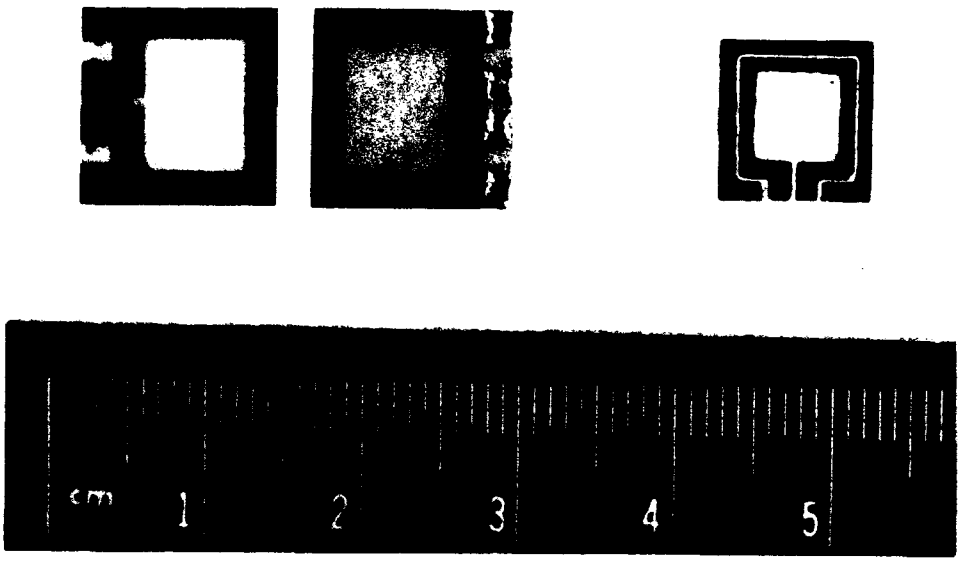

Figure 15. Prototype planar transformers made from a melt-processed $Bi_2Sr_2CaCu_2O_8$ thick film (right), and two $YBa_2Cu_3O_7$ thin films (left).

The resistance versus temperature characteristics of each loop of this prototype transformer are shown in figure 16. The outer loop will be referred to as the primary, and the inner loop as the secondary. The dc resistance between the two loops is greater than 30 MΩ. The zero resistance T_c of both loops is 80 K. The ac characteristics of this transformer were measured using a Princeton Applied Research 124A lock-in amplifier and a Hewlett-Packard 54501A digitizing oscilloscope. The input to the oscilloscope was taken from the signal monitor output of the lock-in. The primary current was determined by measuring the voltage across a small resistor (on the order of 1 Ω) placed in series with the primary. A schematic of the circuit used is shown in figure 17, where the + and − signs refer to the lock-in input polarity. Figure 18 shows the primary current, primary voltage, and secondary voltage waveforms for the transformer when operated at a temperature of 13.8 K and a frequency of 10 kHz. Note that the voltage leads the current in the primary by 90°, as expected from equation 6. Knowing the frequency, the amplitudes of these primary signals give, based on equation 6, a primary inductance value of 12 nH. Operation at the same frequency at 77.3 K is shown in figure 19. The waveforms in these figures have been averaged over 32 sweeps by the oscilloscope.

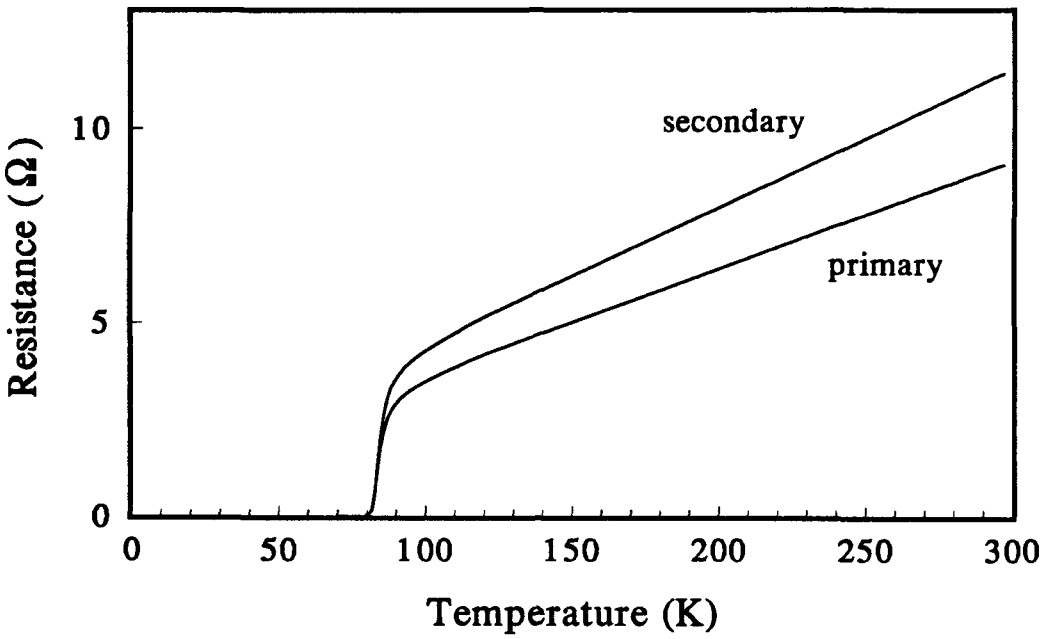

Figure 16. Resistance versus temperature of the primary and secondary loops of the $Bi_2Sr_2CaCu_2O_8$ thick film transformer shown in figure 15. The film resistivity at 300 K is 2.9 mΩ-cm.

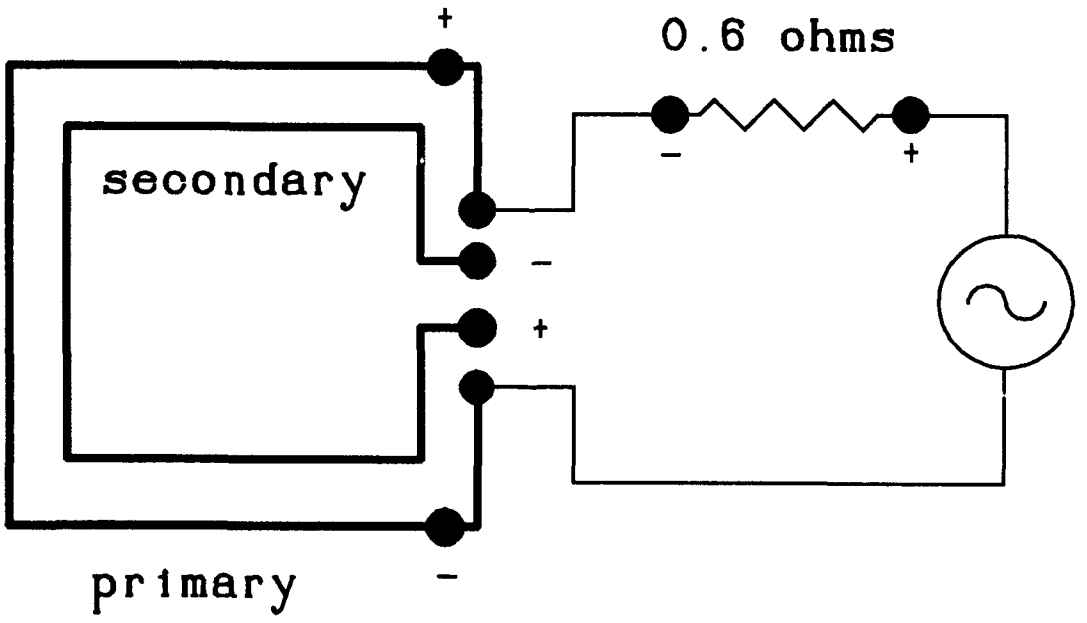

Figure 17. Schematic representation of the connections used for the ac measurements of the $Bi_2Sr_2CaCu_2O_8$ thick film transformer.

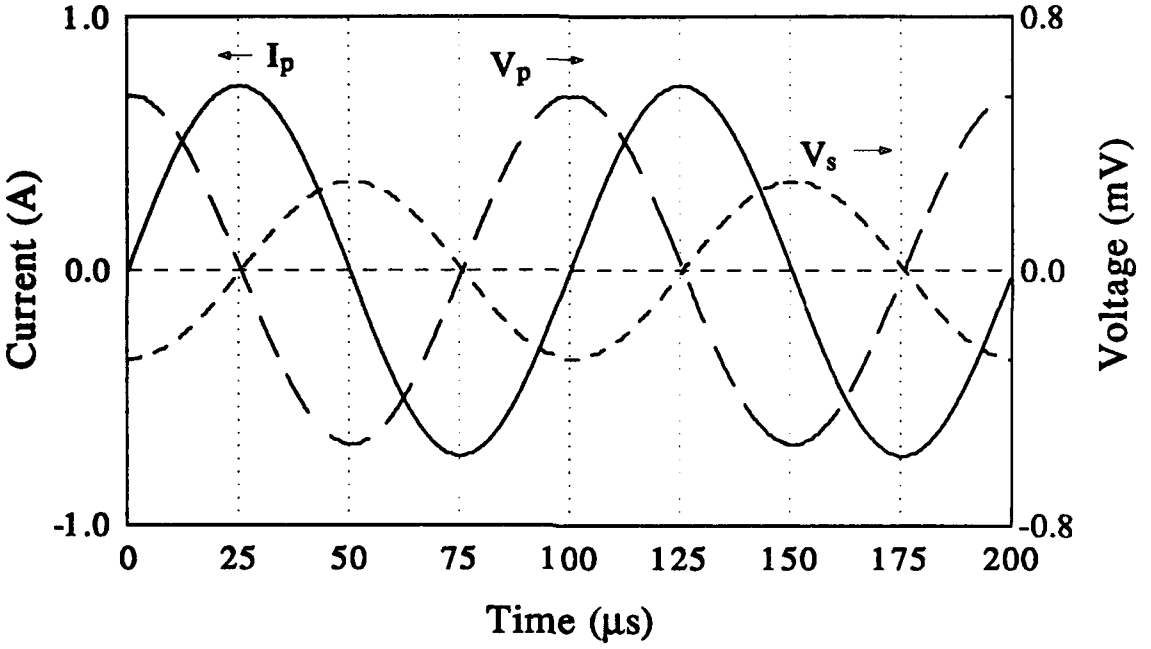

Figure 18. Primary current I_p, primary voltage V_P, and secondary voltage V_s of $Bi_2Sr_2CaCu_2O_8$ thick film transformer operated at a frequency of 10 kHz and a temperature of 13 K.

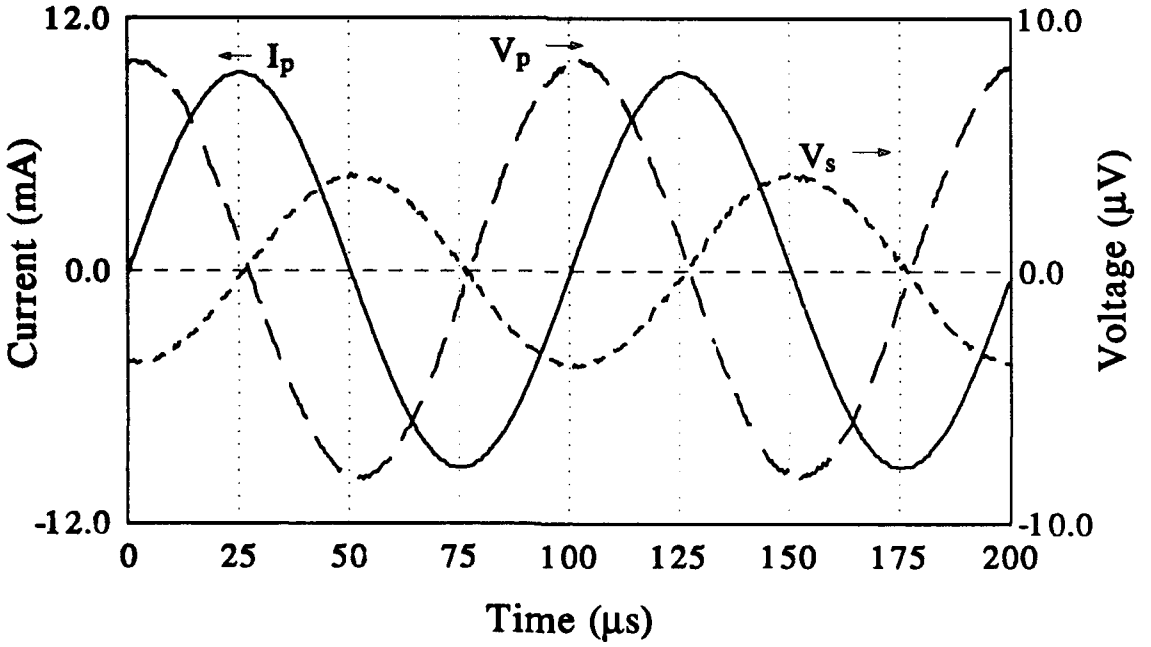

Figure 19. Primary current I_p, primary voltage V_P, and secondary voltage V_s of $Bi_2Sr_2CaCu_2O_8$ thick film transformer operated at a frequency of 10 kHz and a temperature of 77 K.

4.3 $YBa_2Cu_3O_7$ THIN FILM TRANSFORMER

A simple prototype transformer was also made using two $YBa_2Cu_3O_7$ thin films produced using *ex situ* processing. Two films (FCS-122 and FCS-123), approximately 1 μm thick, were deposited at ambient temperature onto separate 12.7 mm square substrates of (100) $SrTiO_3$ which were masked in an appropriate pattern using Kapton tape and aluminum foil. After removing the masking, the films were postannealed as described in section 3.2. The anneal temperature was 915°C, and the cooling rate from 915°C to 750°C was 5°C/min. Gold pads, approximately 5000 Å thick, were sputtered onto the current and voltage contact areas of the films. The films, with pads, were annealed in O_2 at 500°C for 30 minutes, at 450°C for 15 minutes, and then cooled to room temperature at 1°C/min. Short pieces of flattened silver wire were attached to the gold pads using In/10% Ag solder. The two substrates were then sandwiched together (film-to-film) separated by a sheet of cigarette paper (to insure electrical insulation) and a thin layer of N-grease (to provide thermal connection). A photograph of the two films (with one substrate flipped over in the "sandwich" orientation) is shown in figure 15. The width of the $YBa_2Cu_3O_7$ lines forming the rectangular loops was 2 mm. The substrates were offset so that the loops overlapped and the contact areas were accessible. The film sandwich was then N-greased to a quartz disk and mounted in the closed-cycle refrigerator, with a differential thermocouple, as described above for the thick film transformer. Twisted pairs of copper wires were soldered to the silver wires for electrical measurements.

The dc resistance versus temperature characteristics of each film are shown in figure 20 (FCS-122 is referred to as the primary and FCS-123 as the secondary). The real and imaginary parts of the ac impedance of film FCS-122, as a function of frequency, are shown in a log-log plot in figure 21. The specific impedance (in Ω-cm) is given by the impedance (in Ω) multiplied by 7.8×10^{-6} cm. The behavior observed in figure 21 is reminiscent of that expected for a simple two-fluid model (see, for example, Van Duzer and Turner, 1981) at frequencies in the MHz and GHz ranges. The two-fluid model, however, cannot account for the relatively large resistance values observed in these films at frequencies of 10^5 Hz or for the leveling-off of the resistance at very low frequencies. The data can be fit, as shown in figure 21 by the solid lines, by an equivalent circuit consisting of a resistor $r = 15$ μΩ in series with a parallel combination of an inductor $L = 17.7$ nH and a resistor $R = 41.3$ mΩ. The impedance Z for such a circuit is given by

$$Z = r + \left[\frac{R}{1 + \left(\frac{R}{\omega L} \right)^2} \right] + i \left[\frac{\omega L}{1 + \left(\frac{\omega L}{R} \right)^2} \right] . \qquad (8)$$

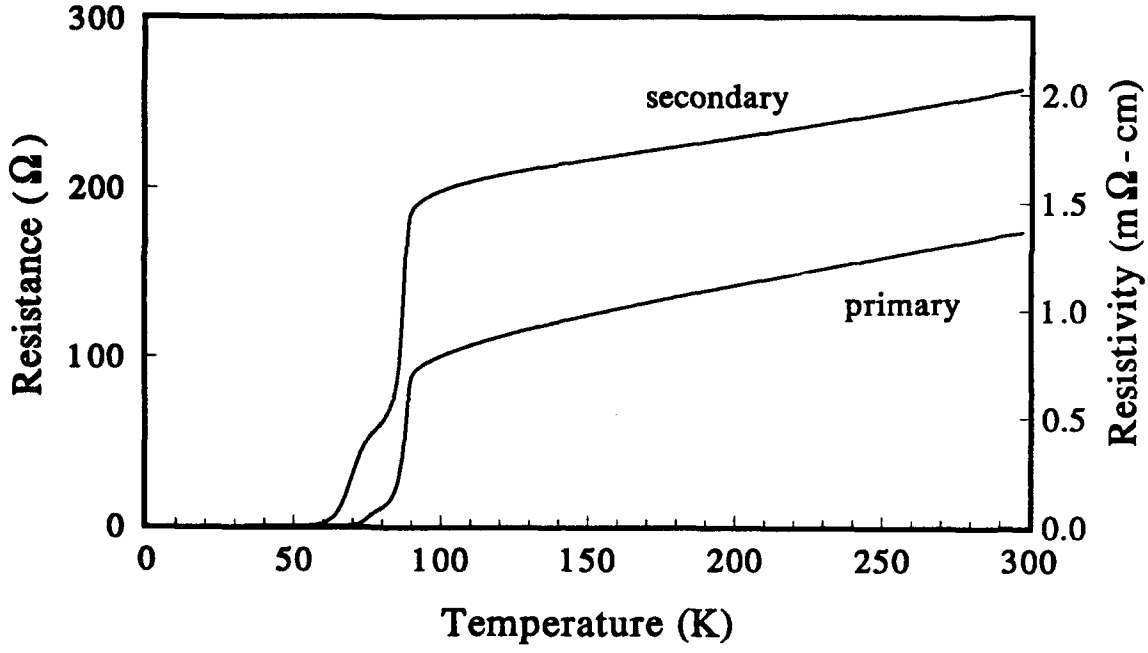

Figure 20. Resistance versus temperature of the primary and secondary loops of the $YBa_2Cu_3O_7$ thin film transformer shown in figure 15.

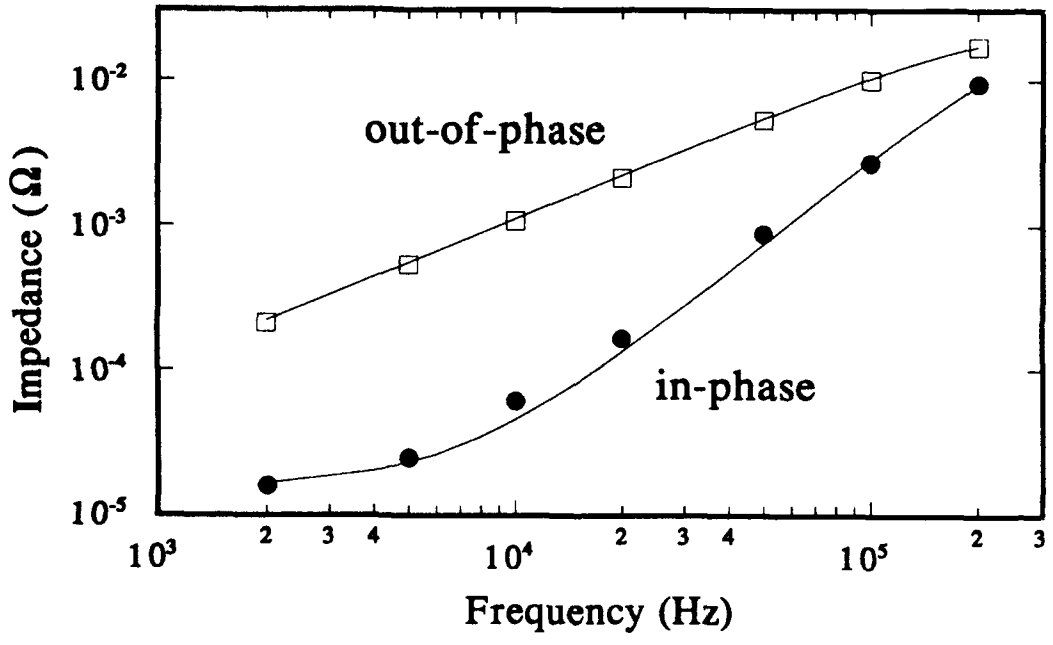

Figure 21. Impedance (in-phase, ●, and out-of-phase, □, with current) versus frequency of primary loop of $YBa_2Cu_3O_7$ thin film transformer at 13 K. Solid lines are least-square fits to an equivalent circuit model (see text).

The geometric inductance for a loop with the dimensions of these films (see figure 15) is estimated to be about 13 nH (Jaycox and Ketchen, 1981). The inductor L in this equivalent circuit most likely corresponds, then, to the superconducting grains forming the film loop. As this film has a quite rough surface (see the SEM micrographs of figure 22), the parallel resistance R might be due to surface resistance of these grains. Since these impedance measurements were made with a (peak-to-peak) current level of 26.3 mA (or about 90% of the critical current at this temperature), it is likely that the series resistance r in this model circuit is due to weak links between grains. These weak links might consist of lower-quality superconductor for which the critical current has been exceeded, or possibly of normal material too thick for tunneling of a super-current.

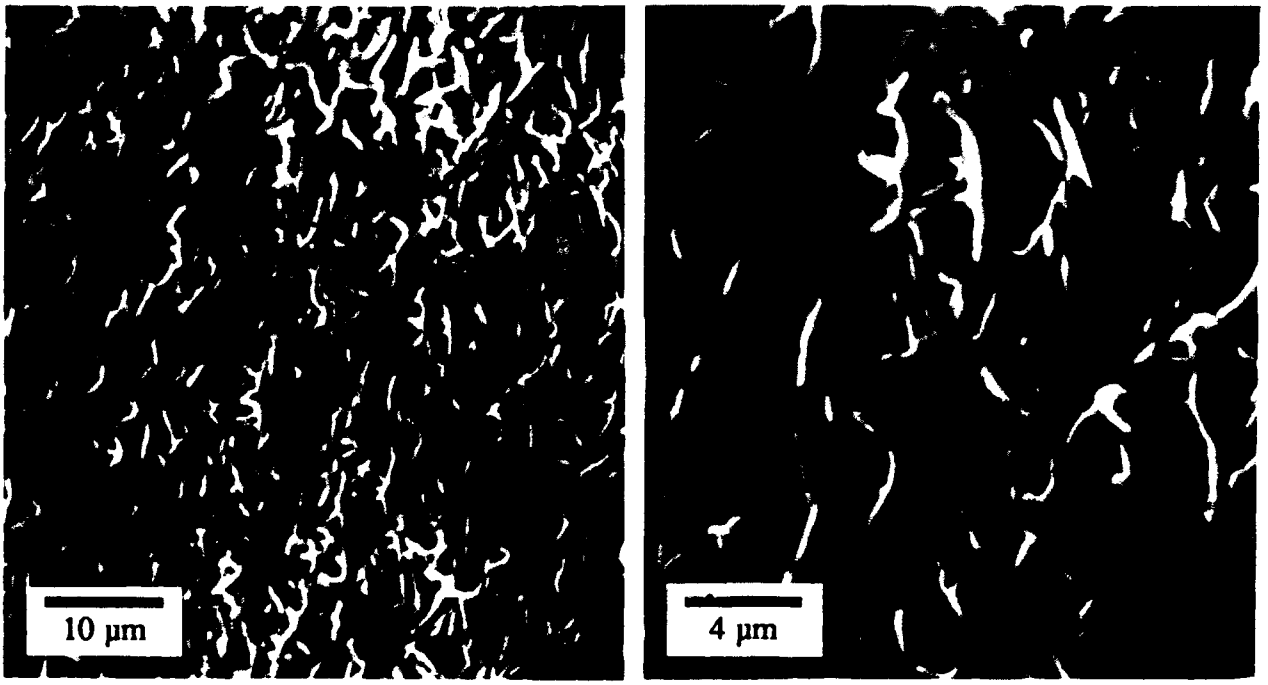

Figure 22. SEM micrographs of $YBa_2Cu_3O_7$ *ex situ* annealed thin film used as the primary loop of the prototype thin film transformer.

As seen from these properties, the $YBa_2Cu_3O_7$ films used for this first prototype are not very high in quality. They have low transition temperatures and critical current densities (J_c = 1.4 kA/cm^2 at 12.9 K for FCS-122). The poor superconducting properties can be attributed to the granular structure of the films, seen in figure 22, which in turn is due to the *ex situ* processing at high temperature. Even so, the film quality is sufficient, as a first step, to illustrate the applicability of high-T_c films to transformer devices.

The ac characteristics of this transformer were measured using a lock-in amplifier and a digitizing oscilloscope, as with the thick film transformer. Figure 23 is a schematic of the circuit used for measurements, again with the + and – signs referring to the lock-in input polarity. The arrows in figure 23 indicate the direction of current when the voltage across the 1 Ω resistor is positive (when only that loop is excited). The currents provided by the sources in both the primary and secondary loops are in phase, while both loops are completely electrically isolated from each other by isolation transformers (not shown). Figure 24 shows the primary current, primary voltage, and secondary voltage waveforms for the transformer at a temperature of 12.9 K and a frequency of 100 kHz. The primary inductance derived from these plots and equation 7 is about 17 nH. In addition to these measurements, the transformer was also operated in a mode where both the primary and the secondary were excited (first separately and then at the same time) while the secondary voltage was measured. As seen in figure 25, the signal induced in the secondary by the primary current is canceled by direct excitation of the secondary. This result rules out the possibility that the "induced" secondary voltage might be due to some spurious signal from some other part of the circuit.

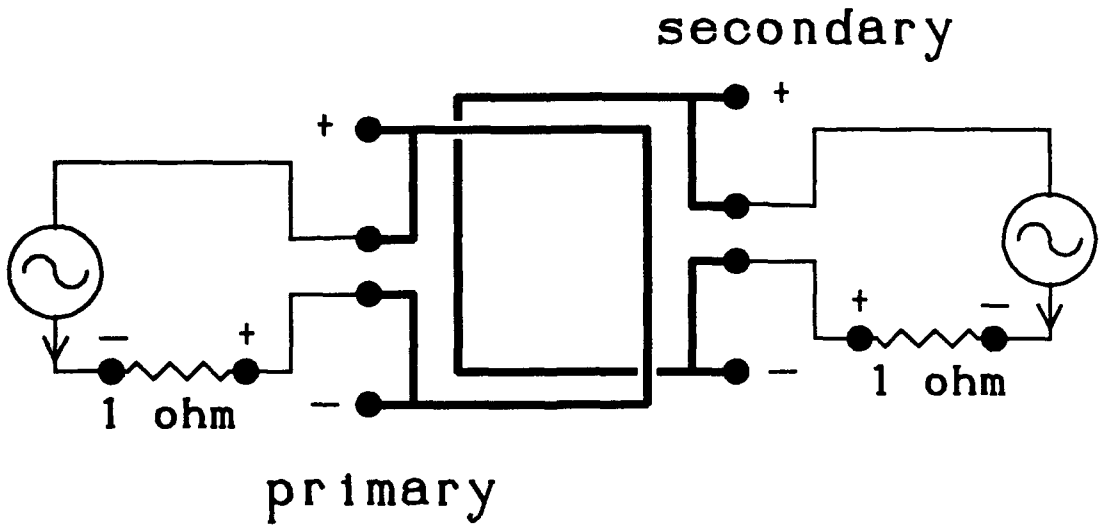

Figure 23. Schematic representation of the connections used for the ac measurements of the $YBa_2Cu_3O_7$ thin film transformer. The current source for the secondary was used only in collecting the data of figure 25.

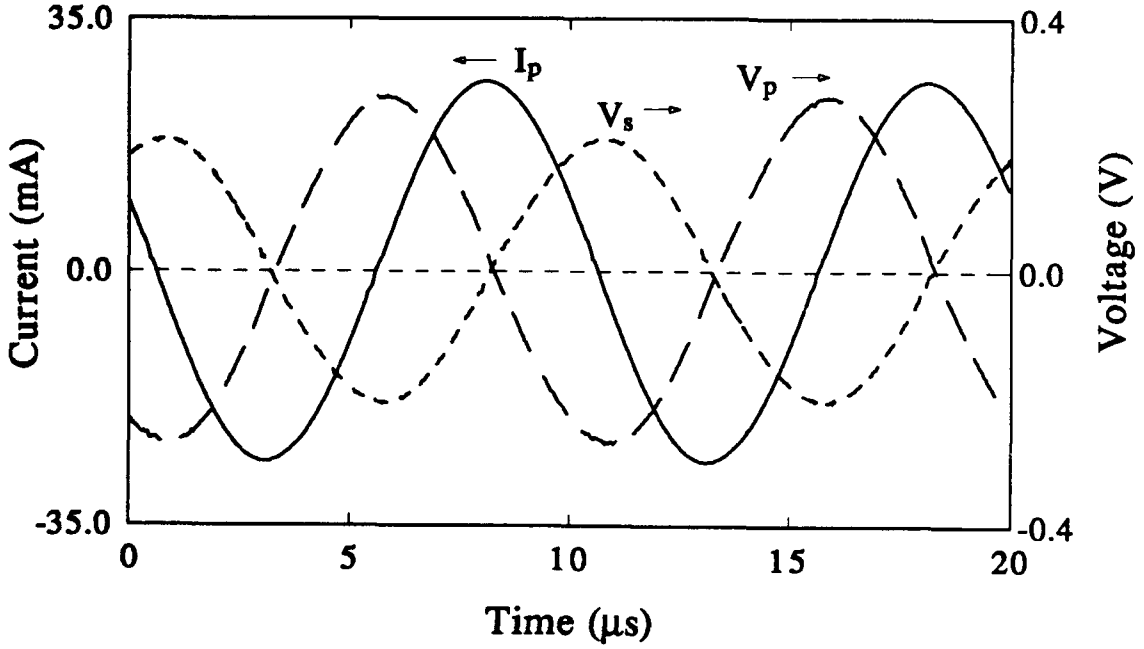

Figure 24. Primary current I_p, primary voltage V_P, and secondary voltage V_s of $YBa_2Cu_3O_7$ thin film transformer operated at a frequency of 100 kHz and a temperature of 13 K.

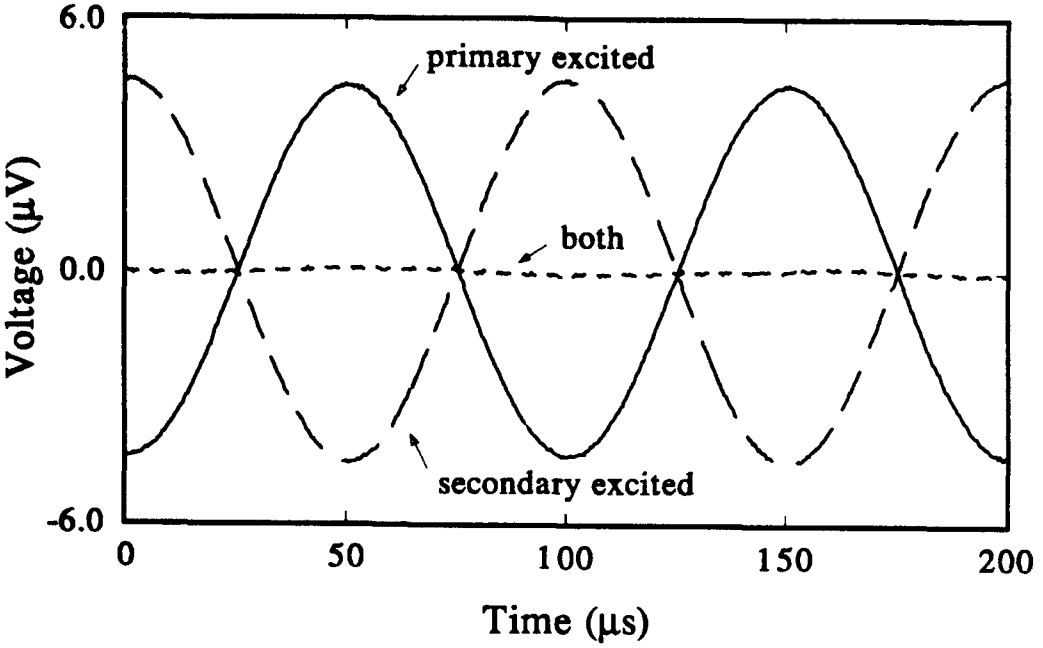

Figure 25. Secondary voltage of $YBa_2Cu_3O_7$ thin film transformer at 13 K with primary only excited (I_p = 4.00 mA RMS), secondary only excited (I_s = 3.82 mA RMS), and both excited.

5. CONCLUSIONS

Two approaches for making high-T_c films for use in a superconducting planar transformer have been pursued: melt-processing of thick films and sputter deposition of thin films. A prototype transformer has been made and characterized using each approach.

The crystalline and superconducting properties of melt-processed $Bi_2Sr_2CaCu_2O_8$ thick films were investigated as a function of melt temperature (895°C to 950°C) and cooling rate (0.1°C/min to 240°C/min) from the melt-processing temperature to the anneal temperature of 850°C. X-ray diffraction measurements indicate that the $Bi_2Sr_2CuO_6$ content increases as the cooling rate is decreased and as the melt temperature is increased. Also from the x-ray data, c-axis alignment increases as the cooling rate is decreased, but decreases with increasing melt temperature. The highest critical currents were obtained for films step-cooled from the lower melt temperatures (900°C). These films also had the lowest $Bi_2Sr_2CuO_6$ content. All films, however, showed the same functional dependence, best described by flux-creep models, of J_c on temperature. The sharp initial decrease and subsequent leveling-off of J_c with magnetic field can be understood in terms of the co-existence of strong and weak links between single-crystal grains.

Thin films of $YBa_2Cu_3O_7$ were deposited by rf diode sputtering, using both *in situ* and *ex situ* techniques. Both employed off-axis sputtering from a single $YBa_2Cu_3O_7$ target. The best *in situ* films in this study to date were deposited at a substrate temperature of 770°C. The best *ex situ* films were post-deposition annealed in O_2 at an anneal temperature of 895 to 915°C (heating up to that temperature in Ar) for one hour, and then cooled to lower temperatures at 5°C/min. Films annealed at around 900°C show greater c-axis alignment than those annealed at lower temperatures. Higher temperatures, however, promote the growth of a second phase with c-axis periodicity of 14.7Å. The content of this phase is reduced, relative to the desired $YBa_2Cu_3O_7$ phase, by longer anneal times and by rapid cooling from the anneal temperature.

A prototype thick film transformer was made by melting $Bi_2Sr_2CaCu_2O_8$ powder on an MgO substrate at a temperature of 900°C. The film was step-cooled after melting, and patterned in the form of two concentric square loops by scribing after melt-processing. A similar square loop transformer was made using two *ex situ* processed thin films of $YBa_2Cu_3O_7$ that were sandwiched back-to-back. Both transformers were operated, with the films in the superconducting state, at frequencies ranging from 1 kHz to 100 kHz (limited only by the available instrumentation). The thick film transformer was operated at temperatures up to 77 K, and at currents up to 1 A.

Planar transformers made from high-T_c films have been demonstrated with two prototype devices. Further optimization of production procedures (particularly for the $YBa_2Cu_3O_7$ thin films) will lead to films with much high critical currents. Practical microelectronic transformers and other inductive devices will require such high-quality films as well as the ability to deposit multiple superconducting and insulating layers.

REFERENCES

Anderson, L.W., and W.W. Beeman. 1973. *Electrical Circuits and Modern Electronics*, Holt, Rinehart and Winston, New York, NY, ch. 5, p. 126.

Anderson, P.W. 1962. "Theory of Flux Creep in Hard Superconductors," *Physical Review Letters*, vol. 9, p. 309.

Bormann, R., and J. Nolting. 1989. "Critical Oxygen Partial Pressure for the "In-Situ" Preparation of High T_c Superconducting Thin Films," *Physica C*, vol. 162-164, p. 81.

Calestani, G., C. Rizzoli, M.G. Francesconi, and G.D. Andreetti. 1989. "The Modulated Structure of $Bi_2Sr_{3-x}Ca_xCu_2O_8$: A Commensurate Model from Single Crystal X-ray Diffraction Data," *Physica C*, vol. 161, p. 598.

Carlson, D.J., M.P. Siegal, J.M. Phillips, T.H. Tiefel, and J.H. Marshall. 1990. "Stoichiometric Effects in Epitaxial $Ba_{2-x}Y_{1-y}Cu_{3-z}O_{7-\delta}$ Thin Films on $LaAlO_3$ (100)," *Journal of Materials Research*, vol. 5, p. 2797.

Chew, N.G., S.W. Goodyear, J.A. Edwards, J.S. Satchell, S.E. Blenkinsop, and R.G. Humphreys. 1990. "Effect of Small Changes in Composition on the Electrical and Structural Properties of $YBa_2Cu_3O_7$ Thin Films," *Applied Physics Letters*, vol. 57, p. 2016.

Dew-Hughes, D. 1988. "Model for Flux Creep in High T_c Superconductors," *Cryogenics*, vol. 28, p. 674.

Dubreuil, D., G. Garry, Y. Lemaitre, L. Rogier, and D. Dieumegard. 1989. "Preparation of High-T_c YBaCuO Thin Films on YSZ and Silicon Substrates by r.f.-Magnetron Sputtering," *Journal of the Less-Common Metals*, vol. 151, p. 303.

Ekin, J.W., H.R. Hart, Jr., and A.R. Gaddipati. 1990. "Transport Critical Current of Aligned Polycrystalline $Y_1Ba_2Cu_3O_{7-\delta}$ and Evidence for a Nonweak-linked Component of Intergranular Current Conduction," *Journal of Applied Physics*, vol. 68, p. 2285.

Ekin, J.W., A.I. Braginski, A.J. Panson, M.A. Janocko, D.W. Capone II, N.J. Zaluzec, B. Flandermeyer, O.F. de Lima, M. Hong, J. Kwo, and S.H. Liou. 1987. "Evidence for Weak

Link and Anisotropy Limitations on the Transport Critical Current in Bulk Polycrystalline $Y_1Ba_2Cu_3O_x$," *Journal of Applied Physics*, vol. 62, p. 4821.

Escribe-Filippini, C., P.L. Reydet, J. Marcus, and M. Brunel. 1989. "Characterization of Sputtered YBaCuO and SmBaCuO Thin Films: Structural Properties and Role of Thermal Treatment," *Journal of the Less-Common Metals*, vol. 151, p. 263.

Farrell, D.E., B.S. Chandrasekhar, M.R. DeGuire, M.M. Fang, V.G. Kogan, J.R. Clem, and D.K. Finnemore. 1987. "Superconducting Properties of Aligned Grains of $Y_1Ba_2Cu_3O_{7-\delta}$," *Physical Review B*, vol. 36, p. 4025.

Feenstra, R., T.B. Lindemer, J.D. Budai, and M.D. Galloway. 1991. "Effect of Oxygen on the Synthesis of $YBa_2Cu_3O_{7-x}$ Thin Films by Post-deposition Annealing," *Journal of Applied Physics*, vol. 69, p. 6569.

Hammond, R.H., and R. Bormann. 1989. "Correlation Between the In Situ Growth Conditions of YBCO Thin Films and the Thermodynamic Stability Criteria," *Physica C*, vol. 162-164, p. 703.

Hampshire, D.P., X. Cai, J. Seuntjens, and D.C. Larbalestier. 1988. "Improved Critical Current Characteristics in 1-2-3 Oxide Superconductors: Weak Flux Pinning and Percolative Aspects," *Superconductor Science and Technology*, vol. 1, p. 12.

Huang, J., T. Li, X. Xie, J. Zhang, T. Chen, and T. Wu. 1988. "A Method to Obtain Superconducting $Y_1Ba_2Cu_3O_{7-y}$ Bulk Material with Strong C-axis Orientation," *Materials Letters*, vol. 6, p. 222.

Jaycox, J.M., and M.B. Ketchen. 1981. "Planar Coupling Scheme for Ultra Low Noise dc SQUIDs," *IEEE Transactions on Magnetics*, vol. MAG-17, p. 400.

Jin, S., T.H. Tiefel, R.C. Sherwood, R.B. van Dover, M.E. Davis, G.W. Kammlott, and R.A. Fastnacht. 1988. "Melt-textured Growth of Polycrystalline $YBa_2Cu_3O_{7-\delta}$ with High Transport J_c at 77 K," *Physical Review B*, vol. 37, p. 7850.

Kapitulnik, A. 1988. "Properties of Films of High-T_c Perovskite Superconductors," *Physica C*, vol. 153-155, p. 520.

Knauf, N., J. Harnischmacher, R. Müller, R. Borowski, B. Roden, and D. Wohlleben. 1991. "Preparation and Characterization of Single-phase Bi-Pb-Sr-Ca-Cu-O High Temperature Superconductors," *Physica C*, vol. 173, p. 414.

Kwak, J.F., E.L. Venturini, and D.S. Ginley. 1987. "The Consequences of Intergrain Josephson Coupling in Ceramic High-temperature Superconductors," *Physica B*, vol. 148, p. 426.

Likharev, K.K. 1979. "Superconducting Weak Links," *Review of Modern Physics*, vol. 51, p. 101.

Martin, S., A.T. Fiory, R.M. Fleming, G.P. Espinosa, and A.S. Cooper. 1989. "Anisotropic Critical Current Density in Superconducting $Bi_2Sr_2CaCu_2O_8$," *Applied Physics Letters*, vol. 54, p. 72.

McGinnis, W.C., E.W. Jacobs, C.D. Rees, and T.E. Jones. 1990. "Pulsed Current Measurement of the Resistive Transition and Critical Current in High T_c Superconductors," *Review of Scientific Instruments*, vol. 61, p. 984.

Murakami, M., M. Morita, K. Doi, and K. Miyamoto. 1989. "A New Process with the Promise of High J_c in Oxide Superconductors," *Japanese Journal of Applied Physics*, vol. 28, p. 1189.

Neumüller, H.W., and G. Ries. 1989. "Critical Currents and Flux Creep in Melt Processed $Bi_2Sr_2CaCu_2O_8$ Superconductor," *Physica C*, vol. 162-164, p. 363.

Onoda, M., A. Yamamoto, E. Takayama-Muromachi, and S. Takekawa. 1988. "Assignment of the Powder X-Ray Diffraction Pattern of Superconductor $Bi_2(Sr,Ca)_{3-x}Cu_2O_y$," *Japanese Journal of Applied Physics*, vol. 27, p. L833.

Peterson, R.L., and J.W. Ekin. 1988. "Josephson-junction Model of Critical Current in Granular $Y_1Ba_2Cu_3O_{7-\delta}$ Superconductors," *Physical Review B*, vol. 37, p. 9848.

Peuckert, M., W. Becker, J. Bock, B. Hettich, H.-W. Neumüller, and M. Schwarz. 1989. "Melt Processing and Oxygen Doping of Bismuth Superconductors," *Physica C*, vol. 162-164, p. 893.

Ryu, J., Y. Huang, C. Vittoria, D.F. Ryder, Jr., J. Marzik, R. Benfer, and W. Spurgeon. 1989. "Effect of Annealing Conditions on the Structural and Superconducting Properties of Y-Ba-

Cu-O Films," *Science and Technology of Thin Film Superconductors*, ed. by R.D. McConnell and S.A. Wolf, Plenum Press, New York, p. 245.

Salama, K., V. Selvamanickam, L. Gao, and K. Sun. 1989. "High Current Density in Bulk $YBa_2Cu_3O_7$ Superconductor," *Applied Physics Letters*, vol. 54, p. 2352.

Savvides, N. 1990. "Flux Creep and Transport Critical Current Density in High-T_c Superconductors," *Physica C*, vol. 165, p. 371.

Shah, S.I., and P.F. Carcia. 1987. "Superconductivity and Resputtering Effects in rf Sputtered $YBa_2Cu_3O_{7-x}$ Thin Films," *Applied Physics Letters*, vol. 51, p. 2146.

Somekh, R.E. 1990. "The Sputter Deposition of Superconducting Ceramics," *Physics and Materials Science of High Temperature Superconductors*, ed. by R. Kossowsky, S. Methfessel, and D. Wohlleben, Kluwer Academic Publishers, Netherlands, p. 327.

Spann, J.R., L.E. Toth, I.K. Lloyd, M. Kahn, M. Chase, B.N. Das, T.L. Francavilla, and M.S. Osofsky. 1990. "Oriented BSCCO Thick Film Coatings on Polycrystalline MgO," *Journal of Materials Research*, vol. 5, p. 1163.

Tallon, J.L., R. G. Buckley, P.W. Gilberd, and M.R. Presland. 1989. "Single-phase Pb-substituted $Bi_{2+y}Ca_{n-1}Sr_2Cu_nO_{2n+4+\delta}$, n = 2 and 3: Structure, T_c and Effects of Oxygen Stoichiometry," *Physica C*, vol. 158, p. 247.

Tanaka, S., and H. Itozaki. 1989. "Crystallinity and Morphology of Superconducting Thin Films Prepared by Sputtering," *Japanese Journal of Applied Physics*, vol. 28, p. L441.

Tarascon, J.M., W.R. McKinnon, P. Barboux, D.M. Hwang, B.G. Bagley, L.H. Greene, G.W. Hull, Y. LePage, N. Stoffel, and M. Giroud. 1988. "Preparation, Structure, and Properties of Superconducting Compound Series $Bi_2Sr_2Ca_{n-1}Cu_nO_y$ with n = 1,2, and 3," *Physical Review B*, vol. 38, p. 8885.

Terada, N., H. Ihara, M. Jo, M. Hirabayashi, Y. Kimura, K. Matsutani, K. Hirata, E. Ohno, R. Sugise, and F. Kasashima. 1988. "Sputter Synthesis of $Ba_2YCu_3O_y$ As-Deposited Superconducting Thin Films from Stoichiometric Target --- A Mechanism of Compositional Deviation and Its Control," *Japanese Journal of Applied Physics*, vol. 27, p. L639.

Tinkham, M. 1975. *Introduction to Superconductivity*, McGraw-Hill, New York, NY, ch. 5, p. 176.

Umezawa, A., G.W. Crabtree, J.Z. Liu, H.W. Weber, W.K. Kwok, L.H. Nunez, T.J. Moran, C.H. Sowers, and H. Claus. 1987. "Enhanced Critical Magnetization Currents Due to Fast Neutron Irradiation in Single-crystal $YBa_2Cu_3O_{7-\delta}$," *Physical Review B*, vol. 36, p. 7151.

Van Duzer, T., and C.W. Turner. 1981. *Principles of Superconductive Devices and Circuits*, Elsevier, New York, NY, ch. 3, p. 125.

Wang, F.R., Q.Z. Wen, C.Y. Li, Y. D. Dai, D. L. Yin, and M.L. Zhou. 1988. "Trapped Flux Effects on Critical Current of Polycrystalline $YBa_2Cu_3O_x$," *Modern Physics Letters B*, vol. 2, p. 613.

Wu, M.K., J.R. Ashburn, C.J. Torng, P.H. Hor, R.L. Meng, L. Gao, Z.J. Huang, Y.Q. Wang, and C.W. Chu. 1987. "Superconductivity at 93 K in a New Mixed-Phase Y-Ba-Cu-O Compound System at Ambient Pressure," *Physical Review Letters*, vol. 48, p. 908.

Yamamoto, K., B.M. Lairson, C.B. Eom, R.H. Hammond, J.C. Bravman, and T.H. Geballe. 1990. "Role of Atomic Oxygen Produced by an Electron Cyclotron Resonance Plasma in the Oxidation of $YBa_2Cu_3O_{7-x}$ Thin Films Studied by *In Situ* Resistivity Measurement," *Applied Physics Letters*, vol. 57, p. 1936.

Zhu, W., M.M. Miller, P.A. Metcalf, C.S. Calhoun, and H. Sato. 1988. "Preparation of Superconducting Films of Bi-Sr-Ca-Cu Oxides by In-situ Melting," *Materials Letters*, vol. 7, p. 247.

APPENDIX A: $J_c(T)$ IN THE FLUX-CREEP MODEL

Equation 1 was derived from the expression for the thermally-activated creep velocity of a flux line (Anderson, 1962; Tinkham, 1975; Dew-Hughes, 1988):

$$v = v_o \exp\left(-\frac{U}{kT}\right) \sinh\left(\frac{W}{kT}\right) \quad , \tag{A-1}$$

where v_o is the flux line drift velocity in the absence of pinning, U is the potential well depth of a pinning site (difference in energy when the flux line is at the pinning site and when it is not at the pinning site), and W is the work done by the Lorentz force F_L between the transport current and each flux line in shifting the flux line lattice from one stable configuration to the next. In the case of zero applied field, the type-II superconductor enters the mixed state when the self-field B generated by the transport current exceeds the lower critical field. Magnetic field lines, each containing one flux quantum Φ_o, penetrate the sample, forming a flux line lattice with spacing $a = (\Phi_o / B)^{1/2}$. These flux lines will move in the sample under the opposing influences of the Lorentz force and pinning.

The electric field induced in the sample by the flux line motion is given by $E = vB = v\beta J$, where the self-field B is proportional to the current density J. At the critical current density J_c, defined by the electric field criterion value E_c, the flux-creep velocity is $v = E_c / (\beta J_c)$. Equation A-1 can be rewritten as

$$\frac{E_c}{v_o \beta J_c} = \exp\left(-\frac{U}{kT}\right) \sinh\left(\frac{W}{kT}\right) \quad . \tag{A-2}$$

The work W can be written as $W = F_L d$, where d is the distance moved by the flux line. Now F_L is given by the force per unit volume of vortex times the volume of vortex on which the force is exerted, or

$$\begin{aligned} F_L &= (J_c b)\ (\pi r^2 p) \\ &= \left(J_c \frac{\Phi_o}{\pi r^2}\right)(\pi r^2 p) \\ F_L &= J_c \Phi_o\, p \quad , \end{aligned} \tag{A-3}$$

where b is the magnetic flux density in a vortex, r is the vortex radius, and p is the length of vortex over which the force is acting, here assumed to be the distance between pinning sites. That is, the force per unit length of vortex is just $J_c\Phi_o$. The distance d moved by the vortex depends on the relative value of the vortex lattice spacing, a, and the distance between pinning sites, p. For $a<p$ (high field or low pinning site density), $d=a=[\Phi_o/(\beta J)]^{1/2}$, while for $a>p$ (low field or high pinning site density), $d=p$. The work done by the Lorentz force is then

$$W = \begin{cases} p\,\Phi_o^{3/2}\left(\dfrac{J}{\beta}\right)^{1/2}, & a<p \\ p^2\Phi_o\,J, & a>p \end{cases} \qquad \text{(A-4)}$$

The pinning energy U is given by the vortex energy per unit volume times the volume of vortex within the pinning site, or

$$U = \left(\frac{H_c^2}{8\pi}\right)(\pi r^2 D) = \frac{H_c^2 r^2 D}{8}, \qquad \text{(A-5)}$$

where H_c is the thermodynamic critical field and D is the extent of the pinning site (assumed to be larger than r).

The temperature dependence of J_c is therefore determined by the temperature dependence of the pinning energy of equation A-5. From the two-fluid, or Gorter-Casimir, model of superconductivity, and from empirical results, $H_c \sim 1-t^2$. The vortex radius r is taken to be the Ginzburg-Landau coherence length ξ, which near T_c depends on temperature as $\xi \sim [(1+t^2)/(1-t^2)]^{1/2}$. Equation 1 is then obtained by combining these expressions with equations A-2, A-4 with $a<p$, and A-5.

REPORT DOCUMENTATION PAGE

Form Approved
OMB No. 0704-0188

1. AGENCY USE ONLY *(Leave blank)*	2. REPORT DATE	3. REPORT TYPE AND DATES COVERED
	January 1992	Final: Sep 1988—Oct 1991

4. TITLE AND SUBTITLE
PROTOTYPE SUPERCONDUCTING PLANAR TRANSFORMERS USING HIGH-T_c THIN AND THICK FILMS

5. FUNDING NUMBERS
PE: 0602936N
PROJ: RV36I21
SUBPROJ: ZE76-01
ACC: DN309050

6. AUTHOR(S)
W. C. McGinnis, J. S. Briggs, T. E. Jones, and L. J. Johnson

7. PERFORMING ORGANIZATION NAME(S) AND ADDRESS(ES)
Naval Ocean Systems Center
San Diego, CA 92152–5000

8. PERFORMING ORGANIZATION REPORT NUMBER
NOSC TR 1479

9. SPONSORING/MONITORING AGENCY NAME(S) AND ADDRESS(ES)
Office of the Chief of Naval Research (OCNR-10P)
Independent Exploratory Development Programs
Arlington, VA 22217–5000

10. SPONSORING/MONITORING AGENCY REPORT NUMBER

11. SUPPLEMENTARY NOTES

12a. DISTRIBUTION/AVAILABILITY STATEMENT
Approved for public release; distribution is unlimited.

12b. DISTRIBUTION CODE

13. ABSTRACT *(Maximum 200 words)*

This report describes a prototype on-chip electrical transformer that was developed using high-transition-temperature superconducting films. Two approaches for making high-T_c films were pursued: melt-processing of thick films and sputter deposition of thin films.

It is concluded that further optimization of production procedures (particularly for $YBa_2Cu_3O_7$ thin films) will lead to films with much higher critical currents. Practical microelectronic transformers and other inductive devices will require such high-quality films as well as the ability to deposit multiple superconducting and insulating layers.

14. SUBJECT TERMS
thin films
superconducting
sputter deposition
melt-processing

15. NUMBER OF PAGES
46

16. PRICE CODE

17. SECURITY CLASSIFICATION OF REPORT	18. SECURITY CLASSIFICATION OF THIS PAGE	19. SECURITY CLASSIFICATION OF ABSTRACT	20. LIMITATION OF ABSTRACT
UNCLASSIFIED	UNCLASSIFIED	UNCLASSIFIED	SAME AS REPORT

21a. NAME OF RESPONSIBLE INDIVIDUAL	21b. TELEPHONE *(Include Area Code)*	21c. OFFICE SYMBOL
W. C. McGinnis	(619) 553–5610	Code 573

INITIAL DISTRIBUTION

Code 014	W. T. Rasmussen	(1)
Code 0141	A. Gordon	(1)
Code 0142	K. J. Campbell	(1)
Code 0143	R. R. Kolesar	(1)
Code 0144	R. November	(1)
Code 144	V. Ware	(1)
Code 50	H. Porter	(1)
Code 501	I. Lagnado	(1)
Code 57	R. H. Moore	(1)
Code 573	J. C. Hicks	(1)
Code 573	W. C. McGinnis	(50)
Code 711	E. F. Rynne	(1)

Defense Technical Information Center
Alexandria, VA 22304-6145 (4)

NCCOSC Washington Liaison Office
Washington, DC 20363-5101

Center for Naval Analyses
Alexandria, VA 22302-0268

Naval Acquisition, Research, & Development
Information Center (NARDIC)
Washington, DC 20360-5000